

AN INVESTIGATION OF ON-CHIP ANTENNA CHARACTERISTICS RELATED TO  
ENERGY HARVESTING APPLICATIONS

by

Dmitry Gorodetsky

B.Sc. in Electrical Engineering, University of Pittsburgh, 1999

Submitted to the Graduate Faculty of  
the School of Engineering in partial fulfillment  
of the requirements for the degree of  
Master of Science in Electrical Engineering

University of Pittsburgh

2002

UNIVERSITY OF PITTSBURGH

SCHOOL OF ENGINEERING

This dissertation was presented

by

Dmitry Gorodetsky

---

It was defended on

May 3, 2002

---

and approved by

Dr. Marlin H. Mickle, Professor, Electrical Engineering

---

Dr. Raymond R. Hoare, Assistant Professor, Electrical  
Engineering

---

Dr. J.T. Cain, Professor, Electrical Engineering

---

Dr. Ronald G. Hoelzeman, Associate Professor, Electrical  
Engineering

---

Dr. Marlin H. Mickle  
Dissertation Director

---

## ABSTRACT

### **AN INVESTIGATION OF ON-CHIP ANTENNA CHARACTERISTICS RELATED TO ENERGY HARVESTING APPLICATIONS**

Dmitry Gorodetsky, M.Sc.

University of Pittsburgh, 2002

The way a certain antenna operates is highly dependent on the dielectric medium in which it is placed. Dielectric media can be characterized by their dielectric constant, which is also called relative permittivity. When no electric field is applied, the positive and negative charges of the dielectric molecules are evenly distributed. Application of an electric field disrupts this balance and results in the creation of dipoles. The number of dipoles that are created is proportional to the permittivity of the dielectric. Permittivity is a measure of the sensitivity of the material to an applied electric field. Stated another way, permittivity is a measure of how much energy can be stored in the electric field.

This thesis reports the research on several types of on-the-chip antennas such as a rectangular spiral and a rectangular patch. The characteristics of these antennas that are useful to Energy Harvesting are analyzed and the effects of permittivity changes in the dielectrics surrounding the antenna are studied.

## TABLE OF CONTENTS

1.0	Introduction.....	1
1.1	Motivation.....	1
1.2	RFID Basics.....	1
1.3	CMOS Process.....	2
1.4	Small Antennas.....	3
1.5	Size and Application Limitations.....	5
2.0	Statement of the Problem.....	6
3.0	Antenna Fundamentals.....	7
3.1	Radiation Pattern.....	7
3.2	Radiation Intensity, Directivity, and Gain.....	10
3.3	Efficiency.....	11
3.4	Input Impedance.....	11
3.5	Bandwidth.....	13
4.0	CMOS Process Fundamentals.....	15
4.1	Physical Geometry.....	15
4.2	Silicon Substrate.....	16
4.3	Oxide.....	17
4.4	Metal.....	18
5.0	Design Tools.....	19
5.1	Ansoft.....	19
5.2	ASITIC.....	25
6.0	Testing Procedures.....	25
6.1	Rig.....	25
6.2	Network Analyzer.....	26
7.0	Patch - Theory.....	26
7.1	Background.....	26
7.2	Frequency.....	29
7.3	Bandwidth and Radiating Efficiency.....	32
8.0	Patch – Simulations.....	33
8.1	Introduction.....	33
8.2	Microstrip with Intrinsic Silicon.....	34
8.3	Microstrip with Doped Silicon.....	38
8.4	Microstrip with Substrate Oxide and Doped Silicon.....	41
8.5	Chip with Sub and Superstrates and Doped Silicon.....	43
8.6	Variation of Superstrate Oxide Permittivity.....	45
8.7	Variation of Substrate Oxide Permittivity.....	46
9.0	Square Spiral – Simulations.....	48
9.1	Introduction.....	48
9.2	Variation of Substrate Oxide Permittivity.....	52

9.3 Variation of Superstrate Oxide Permittivity .....	53
10.0 Summary and Conclusions .....	54
BIBLIOGRAPHY .....	59

## LIST OF FIGURES

Figure 1.1 RFID the old way. ....	2
Figure 1.2 Chip Photograph. ....	2
Figure 1.3 Chip Diagram ....	3
Figure 1.4 Microstrip and On-chip Antennas ....	5
Figure 1.5 Wirebonder ....	6
Figure 3.1 Antenna orientation. ....	8
Figure 3.2 Example 3-D E-Field Pattern ....	9
Figure 3.3 Coordinate System Used with Antennas. ....	14
Figure 4.1 Spiral Ridges ....	16
Figure 4.2 Chip Geometry ....	18
Figure 5.1 Models Possible with Ensemble ....	20
Figure 5.2 Sample 2-D Radiation Pattern ....	21
Figure 5.3 Ensemble Meshing Example ....	22
Figure 5.4 Example of HFSS Meshing. ....	23
Figure 5.5 Port depiction. ....	24
Figure 6.1 Test Rig ....	26
Figure 6.2 Network Analyzer ....	26
Figure 7.1 Patch geometry ....	27
Figure 7.2 Chip Layer Diagram for Patch. ....	29
Figure 8.1 Patch Details (all units in $\mu\text{m}$ ). ....	34
Figure 8.2 Input Impedance ....	35
Figure 8.3 Magnitude of Reflection Coefficient. ....	36
Figure 8.4 Gain Pattern with Undoped Silicon (unitless). ....	37
Figure 8.5 Input Impedance with and without Doping ....	39
Figure 8.6 Gain Pattern with Doped Silicon (unitless). ....	40
Figure 8.7 Geometry for Simulation. ....	41
Figure 8.8 Input Impedance with Substrate Oxide ....	42
Figure 8.9 Geometry for Simulation. ....	43
Figure 8.10 Chip Antenna Input Impedance. ....	44
Figure 8.11 Resonant Frequency as a Function of Superstrate Permittivity. ....	45
Figure 8.12 Input Impedance with Superstrate Permittivity of 13.4. ....	46
Figure 8.13 Resonant Frequency as a Function of Substrate Oxide Permittivity ....	47
Figure 8.14 Input Impedance with Substrate Permittivity of 5.0. ....	48
Figure 9.1 Square Spiral Top View. ....	49
Figure 9.2 Spiral Geometry Side View ....	49
Figure 9.3 Spiral Antenna with a Via to Ground ....	50
Figure 9.4 Effect of Middle Via. ....	50
Figure 9.5 Input Impedance of Spiral Antenna (no via). ....	51

Figure 9.6 Effects of Changing the Substrate Permittivity.....	52
Figure 9.7 Effects of Changing the Superstrate Permittivity.....	53

## **1.0 Introduction**

### **1.1 Motivation**

The motivation for the research that has led to this work has been the demand for smaller and less expensive devices in the radio frequency identification (RFID) arena. RFID involves the identification of items via electromagnetic waves in the RF region of the spectrum. This technology is similar to barcodes but instead of “printed barcodes”, special attachable or embedded tags are placed on or in each object to be identified. The basics of this process are outlined below.

### **1.2 RFID Basics**

The base station or scanner sends an RF signal to power the tag. The remotely powered tag processes certain information and modulates an RF signal that sends back information to the base station. The scanning process with RFID is similar to scanning with barcodes. The disadvantages of barcodes that are remedied by RFID are that the barcode scanner has to be in closer proximity with a more constrained orientation. The location of the barcode must be visible to the scanner. Another advantage of RFID is that the tag placed on each item can be reprogrammed with new information at any point whereas the barcode is only printed once.

In order for the tag to work as outlined above, it must consist of a receiving antenna, some electronics, and a transmitting antenna, which may be shared with the receiving antenna. Using conventional methods [9,10], the antennas and electronics can be placed on a printed circuit board (PCB). Below is an example whose dimensions are 8.2 x 4.4 x 0.2 cm.

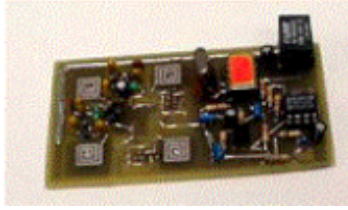


**Figure 1.1** RFID the old way.

The drawbacks of the approach outlined above are the relatively large footprint and power required to run the on-board electronics. Both of these disadvantages can be overcome by combining the antenna and the electronics on a monolithic microwave integrated circuit (MMIC). These ICs or chips as they are commonly called can be produced by MOSIS. The typical ones produced during this research measure roughly 2.2 x 2.2 x 0.4 mm. The reduction in size of the circuitry allows it to work at lower power levels and at a faster speed.

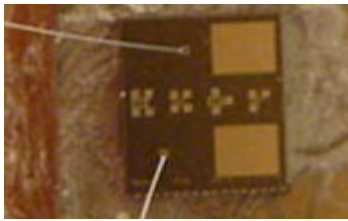


**Figure 1.2** Chip Photograph.

### **1.3 CMOS Process**

The process used to manufacture the antennas on which this thesis is focused is the AMI ABN 1.5  $\mu\text{m}$ . process offered by MOSIS. This process has a 1.5  $\mu\text{m}$ . feature size, up to two metal layers, and up to two polysilicon layers. The feature size refers to the minimum dimension of a metal structure that can be created. The metal layers have thicknesses of 0.6 and 1.0  $\mu\text{m}$ . and are made with aluminum. They are separated by a layer of oxide. Polysilicon is used for the gate of a MOS transistor and is conductive. Polysilicon is placed below the metal layers on the

chip, and it is separated from the metal by an oxide. A second polysilicon layer may also be used. A simplified diagram showing all the possible layers appears below.

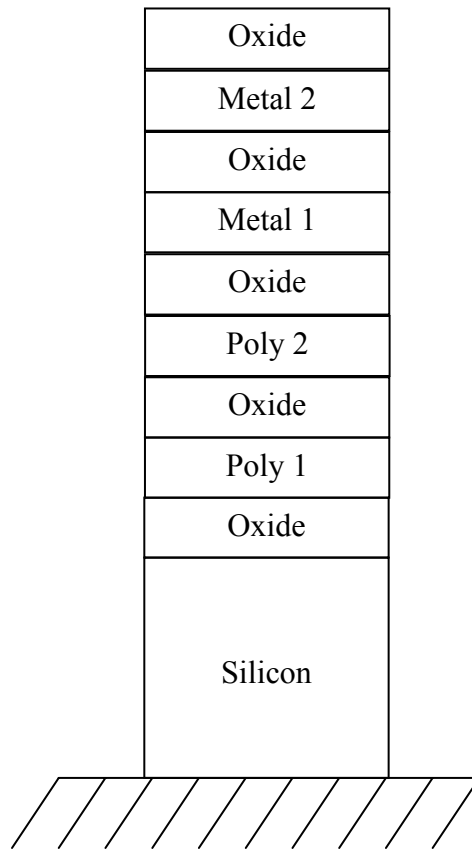


**Figure 1.3** Chip Diagram

#### **1.4 Small Antennas**

As mentioned earlier, inexpensive RFID devices call for the use of small antennas. Small antennas are utilized to keep the tag size down in order to provide many packaging alternatives. Research on similar devices has been done at Berkeley for the Smart Dust project [11]. The main difference between our work is that the mode of communication for Smart Dust is primarily optical whereas that at Pitt is primarily RF. The second difference is that the Smart Dust chips typically require a battery but those reported here use the ambient RF energy

propagated through the air as a source of power. Self-powered nodes are studied in another Berkeley project called “PicoRadio” but instead of RF they use sources such as solar energy, vibrations, and acoustic noise [15]. Investigations of low-power sensing devices similar to Smart Dust are also being conducted at the UCLA Wireless Integrated Network Sensors Project (WINS) and the Ultra Low Power Wireless Sensor Project at MIT [12, 13].

The research in microstrip antennas has been the driving force of the miniaturization of antennas. As mentioned in [5], the trend started with the introduction of microstrip transmission lines in the 1950s. Soon it became very clear that these lines suffered from radiation losses and other parasitic effects, which became worse with frequency. Years later the concept of microstrip antennas emerged where the designer was concerned with maximizing these radiation losses. Microstrip antennas usually have planar configurations. They are very compact and easy to manufacture. One advantage is that because of the antenna’s simple geometry, it can be manufactured in a non-planar configuration to conform to the curved surfaces of objects on which it is mounted [6]. These can be the surfaces of vehicles, missiles, etc. Another attractive advantage of these antennas is that they can easily be manufactured on integrated circuits.

Microstrip antennas are typically fabricated on printed circuit boards (PCB) with a rather simple structure under the antenna. These antennas were initially fabricated as wave guides and found to actually radiate RF energy suggesting an antenna. An antenna on a chip is typically a planar antenna that is placed on a metal layer. This metal layer is located between a protective dielectric above it and two layers of dielectric below it. Under the lowest dielectric layer is the ground plane. This configuration is a special case of microstrip antennas and many of the results useful for microstrip antennas apply to the design of antennas on a chip. However, the structure underneath the antenna on a chip is much more complicated. A typical microstrip antenna

shown in Figure 1.4a has a layer of dielectric sandwiched between a layer of metal and the ground plane. Compare Figure 1.4a with Figure 1.4b to see the difference between a microstrip and an on-chip antenna.

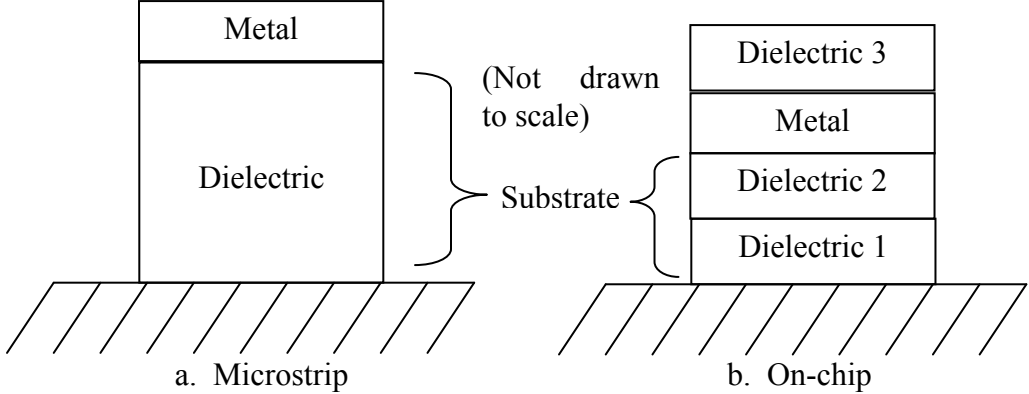


**Figure 1.4** Microstrip and On-chip Antennas

**1.5 Size and Application Limitations**

The chips fabricated with this process have been limited to squares of 2.2 mm. or 4.4 mm. on each side. They are manufactured on a die whose height is no more than 350  $\mu\text{m}$ . The test die come from the foundry in a non-finished form, and a special machine called the wire bonder, shown in Figure 1.5, must be used to connect the pads on the chip to the outside world.



**Figure 1.5** Wirebonder

## **2.0 Statement of the Problem**

The major objective of this thesis is to demonstrate the ability to vary the permittivity of several dielectric layers of a CMOS process to provide design parameters for an antenna on a chip. In particular, the AMI ABN 1.5  $\mu\text{m}$ . process will be used for the purpose of illustration.

The high-frequency rectangular patch and the low-frequency square spiral antennas will be used for the example designs. The variations in permittivity will be illustrated through simulation. The layers whose permittivity will be varied are the substrate oxide and the superstrate oxide. The goal will be to show how the operating frequency of the on-chip antennas can be varied in response to the variations in the permittivities of the different dielectric layers. The design equations for the patch antenna will be presented. The results of modifying the structure for which the equations are designated will be shown, as the structure is transformed

from a microstrip to an on-chip antenna. The permittivity variations in the dielectric layers will also be shown for the spiral antenna.

Permittivity of a dielectric is a measure of its ability to store charge. A change of the relative permittivity of a dielectric surrounding an antenna can be shown to have an effect on the antenna's resonant frequency. In doing this, care must be taken not to disturb the other characteristics that make this structure an antenna.

The indices for evaluation will be the reflection coefficient, the input impedance, antenna gain, and efficiency. Based on the information from the input impedance curves, the antenna's resonant frequency will be extracted.

### **3.0 Antenna Fundamentals**

#### **3.1 Radiation Pattern**

The radiation pattern of an antenna is an important characteristic that will represent graphically one of the radiation properties of the antenna as a function of space coordinates. The properties that can be shown are the power flux density, radiation intensity, field strength, directivity phase, and polarization [1]. Usually these plots are made on a spherical surface of a constant radius  $r$  away from the antenna centered at the origin. The coordinate system used is shown in the figure below, which displays a dipole antenna.

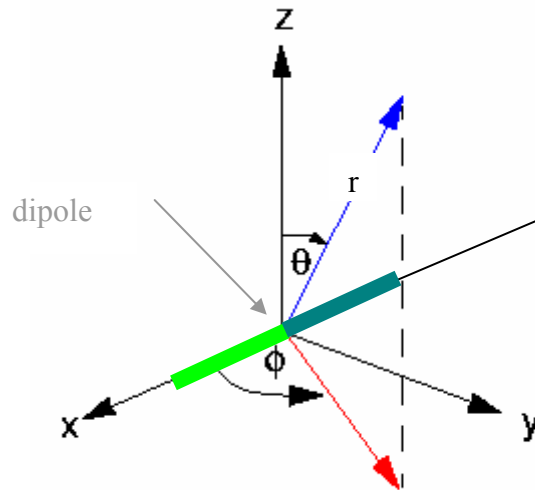


**Figure 3.1** Antenna orientation.

There are three ways that the values corresponding to a surface can be illustrated for a differential element  $dS$  on the surface of the sphere. The simplest way is to use a spectrum of colors that correspond to a range of values and to color each square of area  $dS$ . A second way is to use just one color to fill each square with area  $dS$  but to draw that square at a radius proportional to the value being plotted. And a third way is to combine both methods on one plot. An example of the third method is shown in Figure 3.2 below. If it is not possible to create one of the three dimensional plots described above, then several two-dimensional plots can be made which are the slices of the sphere with one of the angles kept constant.

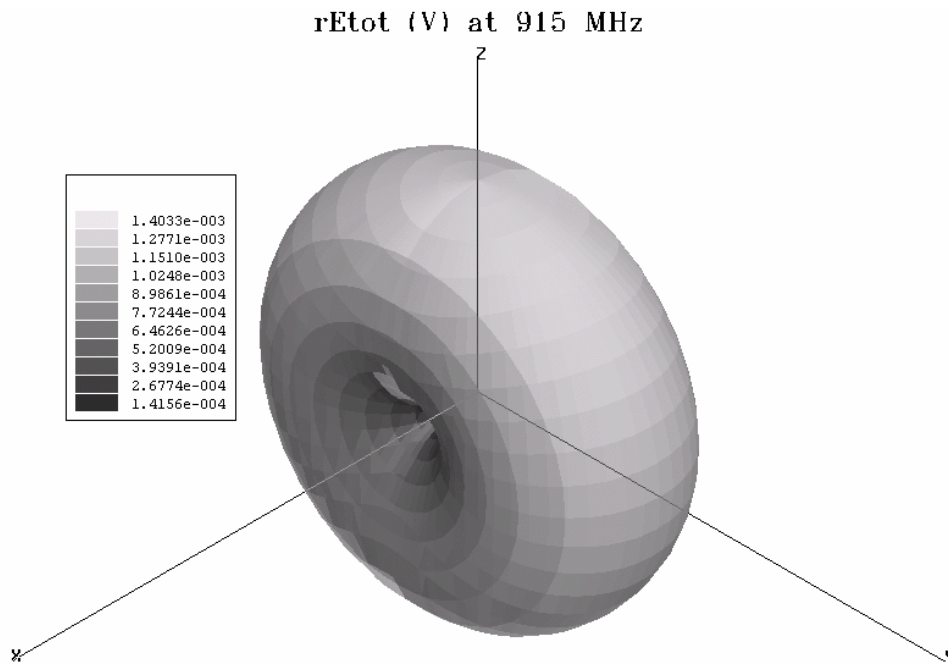


**Figure 3.2** Example 3-D E-Field Pattern

Three regions exist which are characteristic of the field distributions. The first region is the reactive near-field region. The second one is the radiating near-field (Fresnel) region. In these two regions the shape of the pattern will vary with distance from the antenna. As the point of interest moves further away, it will enter the far-field (Fraunhofer) region where the shape of the pattern will no longer vary with distance. The far field region is entered when the distance from the antenna is greater than  $2D^2/\lambda$ , where  $D$  is the maximum overall physical dimension of the antenna [7]. As an example, for one of the antennas reported in this thesis, this distance is 0.00118 inches. For the remainder of this thesis we will only be interested in the far-field region because it lends itself to comparison of patterns resulting from different antennas. This is one of the primary mechanisms of evaluating a particular antenna for RFID designs.

### 3.2 Radiation Intensity, Directivity, and Gain

Balanis defines radiation intensity as “the power radiated from an antenna per unit solid angle.” It is given by:

$$U(\theta, \phi) = r^2 W_{\text{rad}}(r, \theta, \phi) \quad (3-1)$$

where  $W_{\text{rad}}$  is the radiation power density in Watts/m<sup>2</sup>. A solid angle is called a steradian. A spherical surface has  $4\pi$  steradians and to obtain the total power (3-1) is to be integrated over  $4\pi$  steradians. Radiation intensity is measured in Watts/steradian.

Directivity is a parameter that stems from radiation intensity. It is a measure of the radiation intensity per a specific solid angle to the radiation intensity averaged over all directions. Directivity can be expressed as:

$$\begin{aligned} D(\theta, \phi) &= \frac{U(\theta, \phi)}{U_{\text{ave}}} = \frac{4\pi}{P_{\text{rad}}} U(\theta, \phi) \\ &= \frac{4\pi}{\iint_S \mathbf{W}_{\text{rad}}(r, \theta, \phi) \cdot d\mathbf{S}} U(\theta, \phi) = \frac{4\pi}{\iint_{\Omega} U(\theta, \phi) \cdot d\Omega} U(\theta, \phi) \end{aligned} \quad (3-2)$$

where  $\Omega$  represents a steradian and  $P_{\text{rad}}$  is the total power radiated by the antenna. In other words, directivity shows the radiation intensity in a given direction normalized to the average radiation intensity. Directivity is a dimensionless quantity.

Gain is also a parameter that is related to the radiation intensity. The following formula, which is used for computing the gain, is very similar to the formula for directivity.

$$\text{gain}(\theta, \phi) = \frac{4\pi}{P_{\text{in}}} U(\theta, \phi) = kD(\theta, \phi) \quad (3-3)$$

where  $P_{\text{in}} = P_{\text{rad}}/k$  and  $k$  is a constant related to the efficiency of the antenna.

Just like directivity, gain is a dimensionless quantity. It should be clear that a plot of gain would account for the losses of the antenna while a plot of directivity will only show its directional properties.

### 3.3 Efficiency

An antenna will have losses at the feed input terminals and it will also have losses due to the conducting material from which it is constructed and due to the dielectric such as a substrate in a microstrip antenna. Balanis expresses the overall efficiency of the antenna,  $e_o$  by:

$$e_o = e_r e_c e_d \quad (3-4)$$

where

$$e_r = \text{reflection efficiency} = (1 - |\Gamma|^2)$$

$$e_c = \text{conduction efficiency}$$

$$e_d = \text{dielectric efficiency}$$

$$\Gamma = \frac{Z_{IN} - Z_0}{Z_{IN} + Z_0}, \text{ and } Z_{IN} \text{ is the input impedance of the antenna looking into the feed and } Z_0$$

is the characteristic impedance of the feed.

### 3.4 Input Impedance

The antenna input impedance,  $Z_A$ , usually refers to the impedance seen looking into the terminals of the antenna. This is different from  $Z_{IN}$ , because  $Z_{IN} = Z_A + Z_{FEED}$ . The antenna impedance has a real and an imaginary component and is given by:

$$Z_A(f) = R_A(f) + jX_A(f) \quad (3-5)$$

The input resistance, which is the real part of the antenna input impedance, will usually consist of two components,  $R_L$ , the loss resistance of the antenna and  $R_r$ , the radiation resistance of the antenna. According to many authors, these two components appear in series [1, 7, 8].

The maximum power transfer theorem states that in order to obtain maximum power from an antenna, its input impedance ( $Z_{IN}$ ) must be a conjugate of the load's impedance. When this is achieved, half of the power will be absorbed in the antenna and half will be utilized in the load.

After the maximum power transfer theorem has been satisfied, the next step is to limit the power losses within the antenna. This can be done by minimizing  $R_L$  and maximizing  $R_r$ . In other words, this is an adjustment of the efficiency of the antenna.

To compute the impedance seen looking into a lossy feed of length  $L$ , the following formula from transmission line theory is used:

$$Z_{IN} = Z_0 \left[ \frac{Z_A + Z_0 \tanh \gamma L}{Z_0 + Z_A \tanh \gamma L} \right] \quad (3-6)$$

where

$Z_0$  = characteristic impedance of the feed (transmission line)

$Z_A$  = antenna input impedance (defined in (3-5))

$$\gamma = \alpha + j\beta$$

$$\alpha = \omega \sqrt{\frac{\mu\epsilon}{2} \left[ \sqrt{1 + \left[ \frac{\sigma}{\omega\epsilon} \right]^2} - 1 \right]} \quad \beta = \omega \sqrt{\frac{\mu\epsilon}{2} \left[ \sqrt{1 + \left[ \frac{\sigma}{\omega\epsilon} \right]^2} + 1 \right]}$$

After careful analysis of (3-6), it becomes apparent that if the characteristic impedance and the antenna input impedance are equal, the term in brackets becomes unity and the input impedance seen is just  $Z_0$ . In this case the length of the feed becomes irrelevant to the impedance seen at its

terminals. This is the condition of perfect matching of the load to the line. When this occurs, all power is absorbed by the load and there is no reflection. Usually in RF work the transmission lines are designed so that their characteristic impedance is real at the specified frequency. The value of the characteristic impedance is typically 50 or 75 ohms. It is this mechanism that enables the connection of multiple units using standard coaxial cables.

### **3.5 Bandwidth**

The bandwidth specification of an antenna is a concept not as simple as that characteristic of a filter for example. In an antenna there are many properties which were described above such as the radiation pattern, the input impedance, and the efficiency. The variation of these properties with frequency is usually very different from each other. The bandwidth can be specified as a range of frequencies where one of these properties is within limits. For instance, in a dipole antenna the bandwidth is usually determined by the impedance curve since the far field pattern changes less rapidly [7], making it a more difficult criterion to be specified.

For a dipole, the electric field has two components, in the  $r$  and the  $\phi$  directions as was shown in Figure 3.1, which is repeated below.

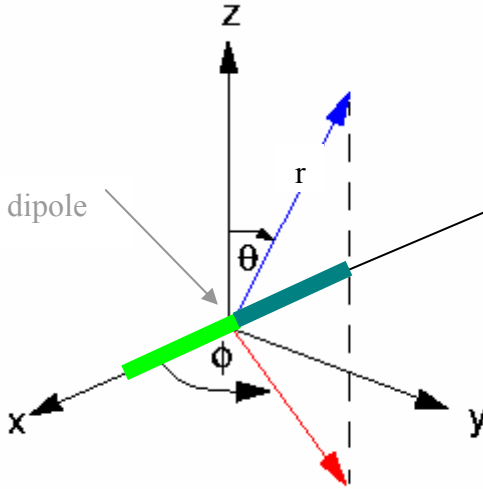


**Figure 3.3** Coordinate System Used with Antennas.

The component in the  $r$  direction is only significant at near field because it becomes negligible in the far field. The component in the  $\phi$  direction is significant in all regions and it is given by [1, 8]:

$$E_{\theta s} = \frac{\eta I_0 dl}{4\pi} \sin\theta \left[ \frac{j\beta}{r} + \frac{1}{r^2} - \frac{j}{\beta r^3} \right] e^{-j\beta r} \quad (3-7)$$

where  $\beta=2\pi/\lambda$  and  $(r,\theta)$  are the coordinates of the point at which the electric field is calculated. The other symbols can be regarded as constants not relevant to this analysis. The time variation is suppressed because it is also not necessary in this analysis.

In the far field region, the  $1/r^2$  and  $1/r^3$  terms become negligible and the equation can be written as:

$$E_{\theta s} = \frac{\eta I_0 dl}{4\pi} \sin\theta \left[ \frac{j2\pi}{r\lambda} \right] e^{-j\beta r} \quad (3-8)$$

Taking the magnitude results in:

$$|E_{\theta s}| = \frac{\eta I_0 dl}{4\pi} \sin\theta \left[ \frac{2\pi}{r\lambda} \right] \quad (3-9)$$

An alternative form for the radiation resistance of the dipole is given in [1, 8] as:

$$R_{rad} = 80\pi^2 \left[ \frac{dl}{\lambda} \right]^2 \quad (3-10)$$

A comparison of (3-9) and (3-10) shows that the electrical field is inversely proportional to the wavelength while the radiation resistance is inversely proportional to the square of the wavelength. Therefore, the variation in the electric field with frequency is slower than it is in the radiation resistance.

The antennas under consideration are to be fabricated on Complementary Metal Oxide Semiconductor (CMOS) chips. The next section presents the necessary background material for the development of the antenna design and simulation on a CMOS chip.

## **4.0 CMOS Process Fundamentals**

### **4.1 Physical Geometry**

The AMI ABN process exists primarily for the manufacture of on-chip CMOS and bipolar transistors. When these transistors are laid out, they require a complex array of layers and manufacturing steps. Since we are interested in laying out planar antennas on one metal layer, the resulting geometry is simpler than that for transistors. Therefore, when we model the patch, the dielectric above it can all be assumed to be at the same height. In the spiral, however, more dielectric will cover the areas that have metal than those areas that don't. This happens because of the technology used in this process. This will result in the top surface of the dielectric having an uneven height.

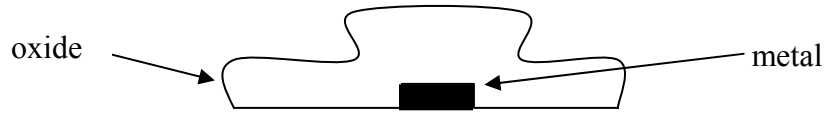


**Figure 4.1** Spiral Ridges

Figure 4.1 shows this situation for only one leg of the spiral, which will occur throughout the spiral's surface. On the average, because the difference in height is small compared to the overall height of the dielectric, this effect will be assumed negligible, and the oxide will be simulated with equal height in all regions. This simplification must be made because the software used to simulate the spiral is not capable of accounting for the ridges.

Two layers of polysilicon are also available to the designer. Polysilicon is heavily doped noncrystalline silicon. Therefore, it is highly conductive. Typically, the gates of MOS transistors are realized with these layers.

## **4.2 Silicon Substrate**

The manufacture of the chip begins with the substrate. Undoped or intrinsic silicon has a lattice structure where each ion is covalently bonded to four other ions. These bonds exist because each silicon ion has four valence electrons. Silicon has many energy bands but the two most important for conduction are the valence band and the conduction band. The valence electrons exist in the valence band. These electrons are weakly bonded and they tend to “jump” to the conduction band if energy is supplied in the form of heat. When an electron is transferred to the conduction band it leaves behind a hole. The symbol for an electron is  $n$  and for a hole it is  $p$ . In an intrinsic semiconductor the concentration of both is the same, and it is  $p = n = 2.0 \cdot 10^{10} \text{ cm}^{-3}$ .

In order to make the primary device for which this process (CMOS) is designed, the MOS transistor, the hole concentration has to be slightly increased, which is done by doping the silicon. Doping refers to a process where a silicon atom is replaced by one having either three or five valence electrons in order to create holes or electrons respectively. Several processing steps later result in a lightly doped p<sup>-</sup> silicon with a hole concentration of  $p = N_A = 2.0 \cdot 10^{16}$  donors•cm<sup>-3</sup>. The electron concentration remains the same.

Another parameter important to our analysis is the hole mobility in the substrate. The velocity with which the hole will move in response to the applied electric field is proportional to hole mobility. The current in turn is proportional to this velocity. This is a form of Ohm's law. For this process the mobility is given as:  $\mu_p = 221.91 \text{ cm}^2 \text{ V}^{-1} \text{ s}^{-1}$ . With availability of these two parameters, the conductivity of the silicon substrate can be calculated as:

$$\sigma = qn\mu_n + qp\mu_p \quad (4-1)$$

The above formula can be simplified because we know that the silicon has been doped with a donor and, therefore, the concentration of holes is much greater than the concentration of electrons. The first term of the formula can be completely eliminated and the resulting conductivity becomes  $71 \text{ siemens} \cdot \text{m}^{-1}$ . The siemens is an SI unit and it is defined as 1 A/V. For purposes of analysis we assume that the silicon substrate is linear, homogeneous, and isotropic [8]. The height of the silicon is nominally 300  $\mu\text{m}$ . Its relative permittivity is typically 11.9.

### 4.3 Oxide

After the substrate has been processed the next step is to deposit several oxides. The first oxide to be deposited is a thick field oxide. This layer is then followed by thin gate oxide. The details of the geometry are shown in Figure 4.2 below.

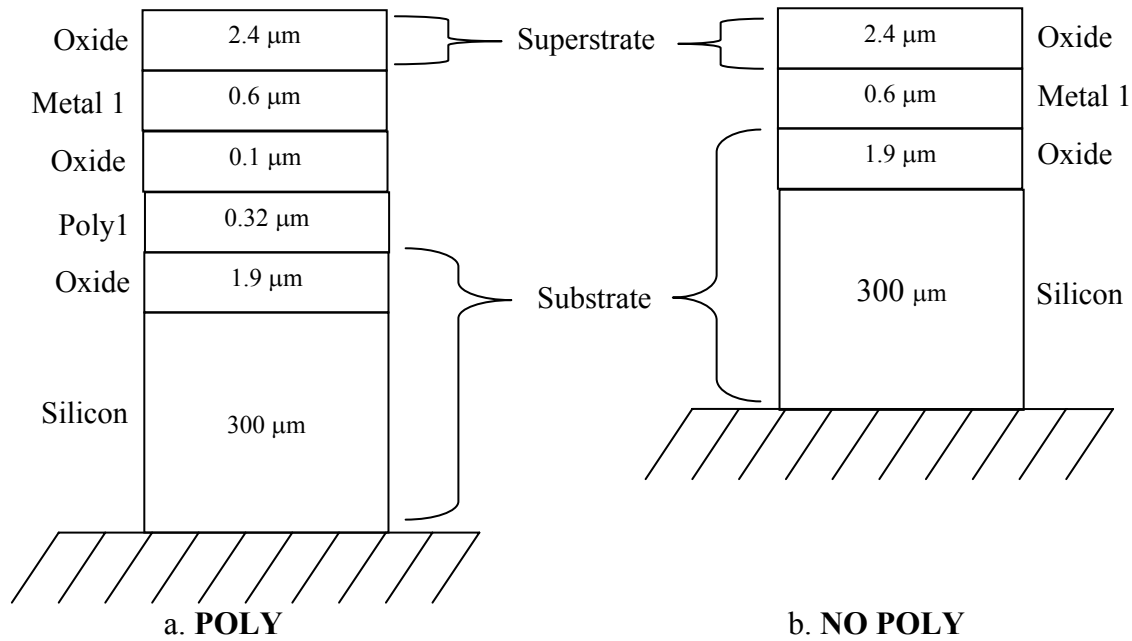


**Figure 4.2** Chip Geometry

The above figure shows the process with only 1 metal layer and 1 poly layer. One additional layer of each is possible, and with each layer there will be slight changes to the geometry. The relative permittivity of the oxide is typically 3.9. It should be kept in mind that oxide separating several layers such as Metal 1 and Poly 1 above will only cover those regions where Poly 1 is present. In the areas where Poly 1 is not present there will be no separation oxide. The result of this will be that the Metal 1 layer will have an uneven height. This will propagate to the top of the chip and cause the development of ridges on as discussed earlier. For purposes of analysis, we assume that the oxide is linear, homogeneous, and isotropic [8].

#### 4.4 Metal

The metal that is used in this process is aluminum. The sheet resistance of the first metal layer, metal 1, is  $0.062 \Omega \cdot \text{square}^{-1}$ . That of metal 2 is  $0.03 \Omega \cdot \text{square}^{-1}$ . The conductivities of these two layers can be calculated with the following formula:

$$\sigma = \frac{1}{R_s H} \quad (4-2)$$

where

$$R_s = \text{sheet resistance } [\Omega \cdot \text{square}^{-1}] \quad H = \text{height of metal [meters]}$$

The effect of sheet resistance becomes clear from the following:

$$R_{Total} = \frac{\rho}{H} \frac{L}{W} = R_s \frac{L}{W} \quad (4-3)$$

where

$$\rho = \sigma^{-1} = \text{resistivity } [\Omega \cdot \text{m} \cdot \text{square}^{-1}]$$

When a choice must be made which metal layer to use, the one with the lower sheet resistance will give the lowest total resistance, i.e. metal 2. To compare the conductivities calculated for the silicon, the conductivity of metal 1 is  $2.69 \cdot 10^7$  siemens $\cdot\text{m}^{-1}$  and that of metal 2 is  $3.33 \cdot 10^7$  siemens $\cdot\text{m}^{-1}$ .

## 5.0 Design Tools

### 5.1 Ansoft

The theoretical analysis involved in the design of some antennas can become quite involved, and in many cases an exact solution may not be possible. This is the point where electromagnetic analysis software comes in. This software provides a graphical display of the radiating characteristics of an antenna as well as the input impedance given by (3-5). A plot at one frequency of interest can be produced or many different frequencies can be swept.

The two programs produced by Ansoft Corporation that are used for dynamic electromagnetic analysis are Ensemble and HFSS. Dynamic quantities are those that vary with

time versus static which do not. As an aside, electromagnetic wave propagation can only be achieved for time-varying electric fields. Static electric fields, analyzed by another Ansoft software product called Maxwell cannot produce electromagnetic waves that propagate through space.

Of the two programs mentioned above, Ensemble is the simplest one to use and understand. It also requires fewer computing resources and simulation time. As shown in the figure below, Ensemble performs analysis of two-dimensional conducting structures with an infinitesimally small thickness. True three-dimensional structures (3D) cannot be simulated. In computerized design this is referred to as 2.5D versus 3D. Structures can be given a finite thickness but this limits the software capability. Also, any number of dielectrics of any thickness surrounding the structure can be included in the analysis.

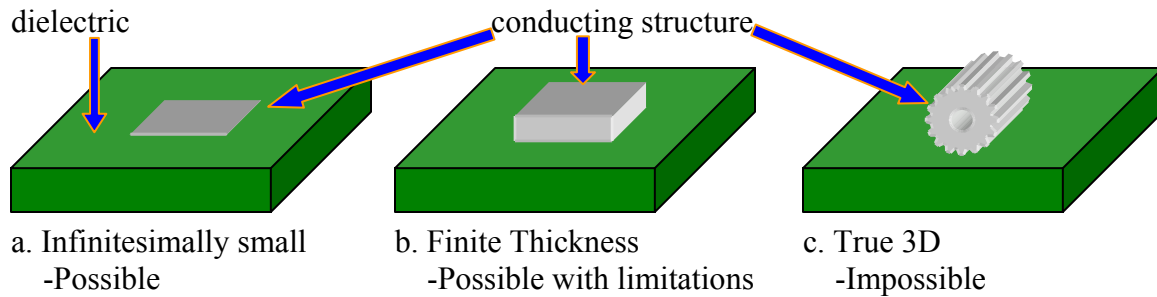


**Figure 5.1** Models Possible with Ensemble

In accordance with the previous discussion of the chip geometry, Ensemble is very well suited to simulate any planar structures on the chip. There is one drawback however. The visualizations of radiated fields are limited to two-dimensional slices of the full sphere discussed in section 3.A. Usually one of the angles (either  $\phi$  or  $\theta$ ) is kept constant while the other one is swept. A sample pattern for a dipole antenna is shown below.

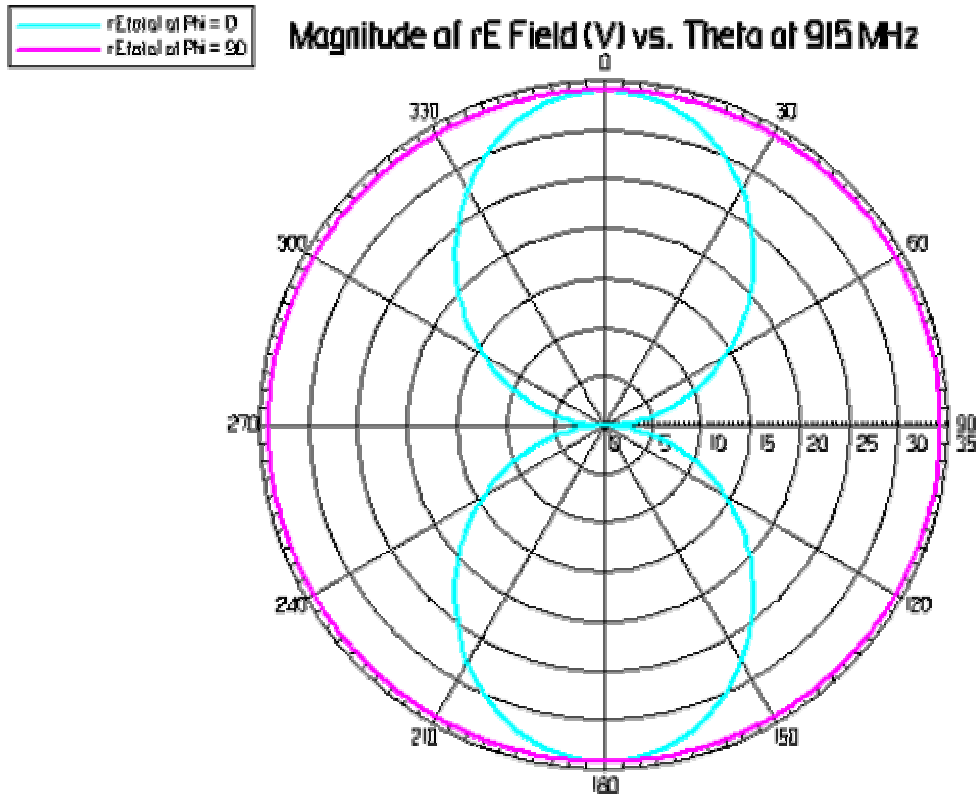


**Figure 5.2** Sample 2-D Radiation Pattern

As can be seen from Figure 5.2, it is possible to display the three-dimensional characteristics of the pattern by varying the angle that is kept constant and performing a new sweep each time. However, this is still a poor substitute for a true three-dimensional display. A spherical plot can be constructed by exporting the field values generated by Ensemble into a custom written computer program. Our research team had developed such program. Ensemble can also display the current and electric field vectors on a plane normal to the plane of the conducting structure.

The simulation performed by Ensemble is done using the method of moments (MOM). This technique, while conceptually simple, is used to solve integral equations instead of differential equations. A mesh consisting of triangles is created on the surface of the structure and the software solves for the currents in each triangle. It then derives all other quantities from

the currents. The mesh can be adaptively refined to generate a more accurate solution. Figure 5.3 below shows the mesh created for a rectangular patch antenna and its feed.

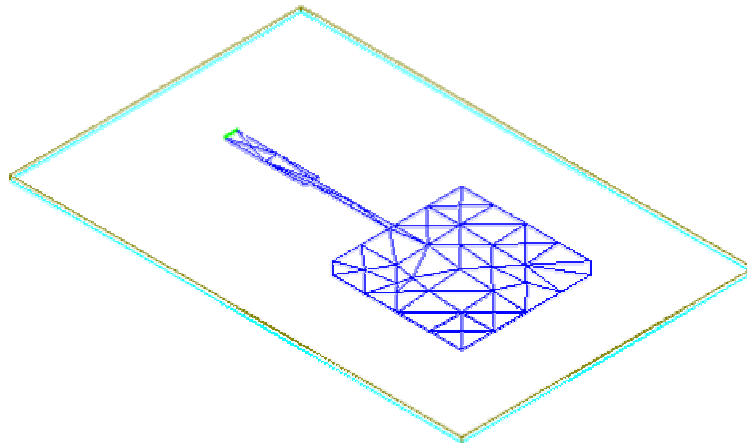


**Figure 5.3** Ensemble Meshing Example

The disadvantages of Ensemble mentioned above are resolved in Ansoft's High Frequency Structure Simulator (HFSS). This software package can simulate any 2-D or 3-D object enclosed in any number of dielectrics. With this program, one is no longer restricted to having a planar structure. Also, the radiation patterns, as well as the current and field vectors, can be shown in all three dimensions.

HFSS uses the finite element method (FEM), which has its origins in structural analysis. This method solves differential equations. The entire volume of the structure (compared with Ensemble which meshes only the surface) is divided into tetrahedrons and the fields are solved within each.

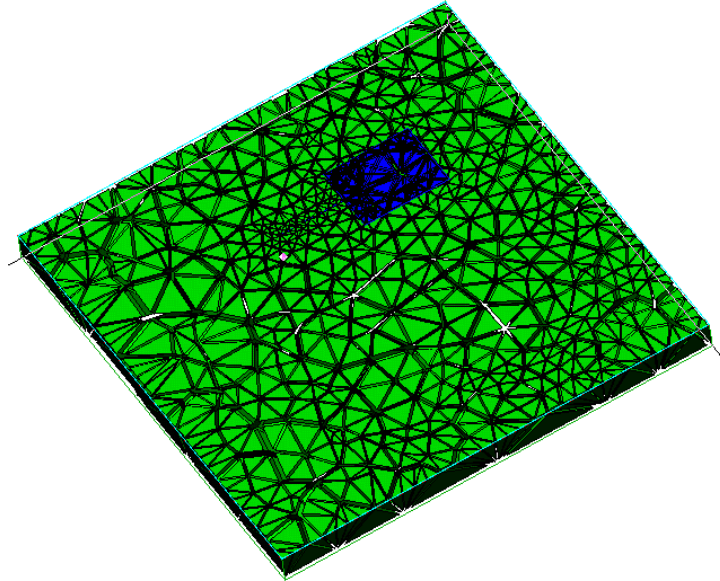


**Figure 5.4** Example of HFSS Meshing

In summary, it should be said that Ensemble is better suited for the simulation of planar structures because it makes certain approximations that simplify the solution and decrease the computing resources used and the computation time. Also, it uses the MOM, which is an approximation in itself because it doesn't solve for any currents inside the volume. HFSS on the other hand is more useful when the structure cannot be represented in a planar way (see Figure 5.1c above) or when a true 3-D plot of the results is required. A useful feature of Ensemble that HFSS lacks is called Optimetrics. This is a software module that allows the program to optimize the geometrical or material properties of the structure until the solution meets one of a set of defined goals.

One type of output generated by both programs is termed the scattering parameters (s-parameters). These parameters are another measure for the input impedance of the structure. In a one-port network they represent the amount of voltage reflected from an imaginary transmission line connected to the structure. The s-parameters can also represent how much voltage is transmitted from one port to another in a two-port network.



**Figure 5.5** Port depiction.

S-parameters were originally invented to characterize the performance of an n-port network. An s-parameter usually has a subscript such as  $S_{mp}$  and it gives the ratio of the phasor voltage at port m due to the phasor voltage at port p, or in other words

$$S_{mp} = \frac{V_m}{V_p} . \quad (5-1)$$

This quantity is a phasor, and it has magnitude and phase information. If the subscripts m and p are different, the s-parameter provides a transmission measurement. This is a convenient measurement for a device such as an amplifier. An antenna, however, typically has only one port and the s-parameter subscripts are the same, i.e.  $m = p = 1$ . In this case the s-parameter provides a reflection measurement. Another name for  $S_{11}$  is the reflection coefficient ( $\Gamma$ ) and it can be written as [16, 17]:

$$S_{11} = \Gamma = \frac{V_{reflected}}{V_{incident}} = \rho \angle \Phi = \frac{Z_A - Z_0}{Z_A + Z_0} \quad (5-2)$$

where

$Z_0$  = characteristic impedance of the imaginary line

$Z_A$  = antenna load impedance

The characteristic impedance of the imaginary transmission line in RF work is usually  $50\Omega$  to facilitate connectivity between distinct RF units. When an antenna is part of a complete circuit, the s-parameters obtained from simulation can be input into yet another Ansoft program called Serenade to perform a system simulation.

## **5.2. ASITIC**

ASITIC is a public domain software package that performs the analysis of passive devices placed on the silicon substrate [14]. ASITIC is an abbreviation for Analysis and Simulation of Inductors and Transformers for Integrated Circuits. ASITIC is a program that is similar to the Ansoft electromagnetic tools in the type of analysis that it performs. However, it has been optimized for designs specifically on a chip and, therefore, it runs faster. This program produces s-parameters or it can produce an equivalent circuit composed of inductors, capacitors, and resistors. The first step in an ASITIC analysis is the creation of Maxwell's equations to describe the structure. Then these equations are converted into a matrix using Green's functions. The matrix is then solved for the currents on the surface of the structure. The program then uses the currents to derive the s-parameters and the equivalent circuit model.

## **6.0 Testing Procedures**

### **6.1 Rig**

A fresh-manufactured chip is received from the foundry with a chip surface to which contacts can be wire bonded. The chip is laid out with special pads to which wire several microns in diameter will be bonded with a wire-bonding machine. The other side of the wire will be connected to a solid contact outside the chip. Since we are dealing with high frequencies, the length of this wire will certainly have an affect on the circuit characteristics. Because of this limitation, a special rig had been designed by our research group for the testing of chips. This rig is a small printed circuit board (PCB), which has a ground layer underneath the chip and locations for inserting SMA connectors. Figure 6.1 illustrates the test chip mounted on the test rig.

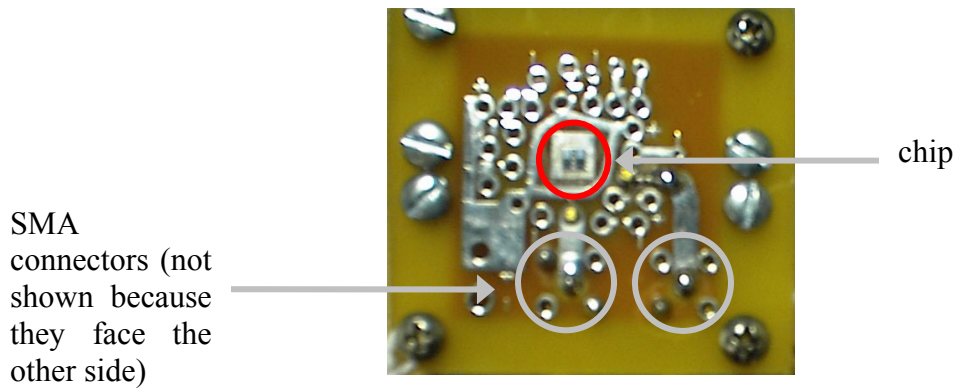


**Figure 6.1** Test Rig

## 6.2 Network Analyzer

After the pads have been bonded to the SMA connectors, the chip can then be tested by connecting cables to the appropriate test equipment. One of the best ways to test an antenna is with a network analyzer. A network analyzer is a device that measures the previously discussed s-parameters.



**Figure 6.2** Network Analyzer

## 7.0 Patch - Theory

### 7.1 Background

In discussing antennas, the input impedance ( $Z_A$ ) of an antenna discussed in Chapter II is an important parameter. The equation for input impedance of a generic antenna is given by[1]:

$$Z_A(f) = R_A + jX_A = (R_r + R_L) + j(X_A + X_i) \quad (7-1)$$

The parameters are defined as follows:

- $R_r$ : Radiation resistance
- $R_L$ : Loss resistance
- $X_A$ : Inductive reactance ( $=\omega L_A$ )
- $X_i$ : Reactance of conductor ( $=\omega L_i$ )

As was mentioned in the Introduction, it is important to minimize the radiation emitted from the feed. To accomplish this task, many different feeding methods have been developed. Some of the most common ones are the probe feed, the coupled feed, and the microstrip feed. The probe feed uses a coaxial probe and is commonly used in circular patches and in rectangular patches to create circular polarization. The coupled feed is located above or below the patch, and it transmits energy onto the antenna without physically touching it. This transmission line uses a substrate different from that used by the patch in order to minimize radiation losses. To simplify the analysis of the concepts of antenna feeds, this thesis will only discuss the microstrip feed of the type shown in Figure 7.1.

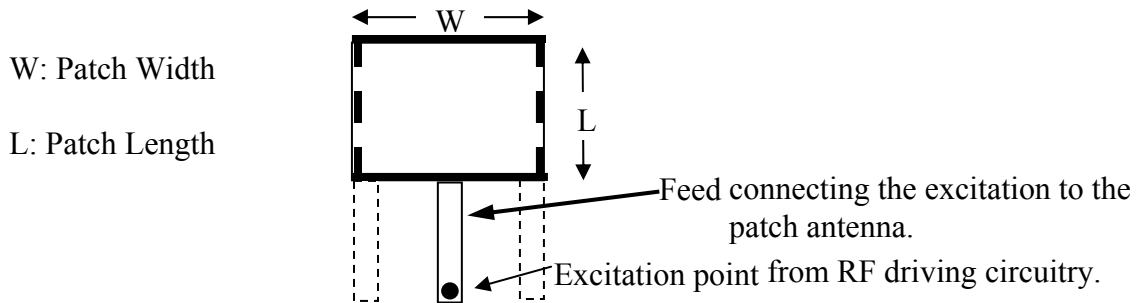


**Figure 7.1** Patch geometry

The feed length and width are very important parameters that will affect the input impedance seen at the excitation point. The location of the feed along the edge of the antenna will also affect the input impedance. As given by [2], the input impedance at resonance will be maximum when the feed point is at either the left or the right edge of the patch, as indicated by

the dashed feeds shown in Figure 7.1. If the feed point is in the middle, as shown by the solid feed in Figure 7.1, the input impedance will be zero. In practice, the feed point will be slightly offset from the center in order to achieve good impedance matching, i.e., maximum power transfer.

The two most common models that are utilized for the analysis of a microstrip patch are the transmission-line and the cavity models. The transmission-line model views the patch antenna as having two radiating slots separated by a length  $L$ , shown by the thick solid lines in Figure 7.1. The slots that are separated by the width  $W$ , shown by the thick dashed lines in the same figure, are neglected because the radiation components emitted from them cancel each other out in the far field. The calculation for the admittance of the first radiating slot is the same as that of the second slot since they have exactly the same dimensions. However, to calculate the total admittance seen at the input, the admittance of the second slot has to be reflected to the input. This becomes challenging mathematically, but it can be simplified when the resonant frequency is reached. At resonance, when  $\lambda=2L$ , the input admittance is given by Balanis as:

$$Y_A(f)=2G_1 \quad (7-2)$$

where the conductance is expressed as:

$$G_1 = \frac{W}{120\lambda_0} \left[ 1 - \frac{1}{24} (k_0 h)^2 \right] = \frac{Wf}{120c} \left[ 1 - \frac{1}{24} 4\pi^2 f^2 \mu_0 \epsilon_0 h^2 \right] \quad \frac{h}{\lambda_0} < \frac{1}{10}$$

in which  $\lambda_0$  is the wavelength in free space and  $h$  is the height of the dielectric.

As mentioned in [5], the feed itself is a radiator and has an effect on the far field radiation pattern produced by the antenna. Because of this the antenna radiation pattern is difficult to control. It is common for half the available power to be lost in the feed. Therefore, a successful

feed/antenna design will seek to minimize the radiation of the feed and maximize the radiation of the antenna at a given frequency.

## 7.2 Frequency

The location of the on-chip antenna layers appears in Figure 7.2. The dimensions show the thickness of each layer. This layering is characteristic of the AMI ABN process. Figure 7.2 shows this process in its simplest form with only one metal layer and no polysilicon layers. This technology can support up to two metal layers separated by an oxide and up to two polysilicon layers also separated by an oxide. If any of these other layers are added, the dimensions will change slightly. However, the substrate thickness will remain the same.

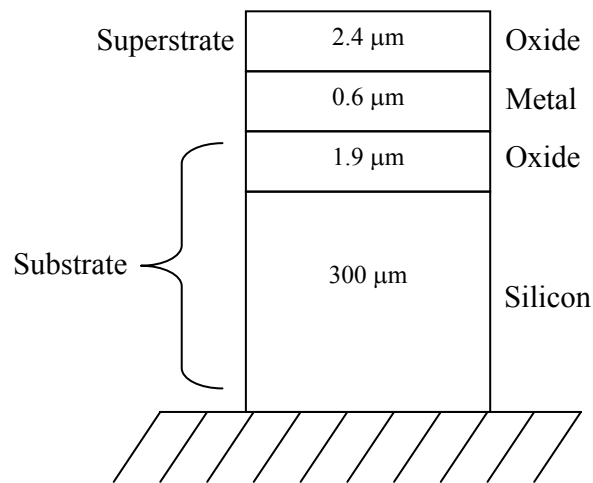


**Figure 7.2** Chip Layer Diagram for Patch.

One primary effect of varying the permittivity of the substrate in a microstrip antenna is to change the resonant frequency.

In its most basic form the rectangular patch typically has two dimensions, the width ( $W$ ) and the length ( $L$ ), as shown in Figure 7.1. Typically the length is the most critical parameter of the patch. The length at which the patch resonates and the input impedance becomes strictly real

is approximately  $\lambda/2$ . The length will be slightly different from half a wavelength because of fringing effects which can be accounted for by  $\Delta L$  given below. When calculating the length, we pretend that the patch is located in a homogeneous dielectric with an effective dielectric constant whose equation is given below as well. For a microstrip patch the length is given by the following formula [1, 18]:

$$L = \frac{c}{2f_r \sqrt{\epsilon_{r,eff}}} - 2\Delta L \quad (7-3)$$

where

$f_r$  is the resonant frequency of the antenna, and  $\epsilon_r$  is the relative permittivity of the dielectric,

$$\epsilon_{r,eff} = \frac{\epsilon_r + 1}{2} + \frac{\epsilon_r - 1}{2} \left[ 1 + 12 \frac{h}{W} \right]^{-\frac{1}{2}} \quad \text{If } \frac{W}{h} \geq 1 \quad (7-3a)$$

$$\epsilon_{r,eff} = \frac{\epsilon_r + 1}{2} + \frac{\epsilon_r - 1}{2} \left[ \left( 1 + 12 \frac{h}{W} \right)^{-\frac{1}{2}} + 0.04 \left( 1 - \frac{W}{h} \right)^2 \right] \quad \text{If } \frac{W}{h} < 1 \quad (7-3b)$$

$$\Delta L = 0.412h \frac{(\epsilon_{r,eff} + 0.3) \left( \frac{W}{h} + 0.264 \right)}{(\epsilon_{r,eff} - 0.258) \left( \frac{W}{h} + 0.8 \right)} \quad (7-3c)$$

The resonant frequency is that frequency at which the antenna exhibits resonance, and the impedance of the antenna is strictly real. The resonant frequency may also be called the resonance frequency or the operating frequency. All these terms mean the same thing and will be used interchangeably throughout this thesis. With simple algebraic manipulation (7-3) can be solved for the resonant frequency as a function of permittivity. This yields:

$$f_r = \frac{c}{2(L + 2\Delta L) \sqrt{\epsilon_{r,eff}}} \quad (7-4)$$

The difficulty with this formula is that it is intended for a microstrip patch with only one dielectric layer. In a patch antenna on a CMOS chip, there exist two dielectric layers between the patch and the ground. These two layers are the oxide and the silicon. Also, there is a layer of oxide above the patch that is called the superstrate. The oxide layer is the one that is directly adjacent to the patch, and the silicon is the one below the oxide. The details of this layering were shown in Figure 7.2. Simulations of the on-chip spiral have shown that the permittivity of the oxide layer has an immediate effect on the resonant frequency of the antenna while the permittivity of the substrate has little or no effect. This result allows us to model the on-chip antenna as being sandwiched between two oxide layers. With this simplification, a relationship similar to the one in (7-3) can be established for an on-chip antenna. In order to obtain this relationship, an expression for the effective relative permittivity of an on-chip antenna has to be derived.

From (7-4), it is seen that the length correction factor, symbolized by  $\Delta L$ , has an effect on the resonant frequency as well. By simple reasoning, from (7-3b), it can be concluded that  $\Delta L$  becomes significant at low values of  $\epsilon_{r,\text{eff}}$ , and high values of the substrate height,  $h$ . For the microstrip patch configuration to be discussed in Section 8.B, the calculated value of  $\epsilon_{r,\text{eff}}$  is 8.64 and the value of  $h$  is  $300 \times 10^{-6}$  m. These values prohibit  $\Delta L$  from being large and, therefore, its effect on the resonant frequency can be neglected.

The width is a less critical parameter because it has a negligible effect on the resonance frequency but affects the efficiency of the antenna. It is given by [1]:

$$W = \frac{c}{2f_r} \sqrt{\frac{2}{\epsilon_r + 1}}. \quad (7-5)$$

### 7.3 Bandwidth and Radiating Efficiency

As stated in [5], for a microstrip antenna the operating bandwidth is proportional to the distance between the antenna and the ground plane. The authors arrive at this conclusion from analyzing the transmission line model of the microstrip patch antenna. Their results are summarized by the following formula for the total-Q factor of a microstrip radiator:

$$Q_T = \frac{2\pi f_r \xi_s}{h(P_r + P_d + P_c)} = \frac{2\pi f_r}{\text{BANDWIDTH}} \quad (7-6)$$

In the above formula, the parameters important to our analysis are:

h: Substrate height                      P<sub>r</sub>: Power radiated by the antenna  
P<sub>d</sub>: Power lost to the dielectric        P<sub>c</sub>: Power lost to the conductor

The formula shows that the bandwidth of a microstrip antenna is proportional to the distance h. The bandwidth is typically given as  $2\pi f_r / Q_T$  [20].

Another consequence of this equation is that the losses increase the bandwidth. The losses however also play a role in another important parameter, the efficiency of the antenna, given by:

$$\eta = \frac{P_r}{P_r + P_d + P_c} \times 100\% \quad (7-7)$$

From the two equations presented in this section, it should be clear that there is a trade-off that must be made between the bandwidth and efficiency of the antenna.

In order to estimate the effect of the substrate permittivity on the bandwidth, (7-4) can be substituted into (7-6). This results in:

$$Q_T = \frac{2\pi f_r \xi_s}{h(P_r + P_d + P_c)} = \frac{c}{2(L + 2\Delta L)\sqrt{\epsilon_{r,eff}}} \frac{2\pi \xi_s}{hP} \quad (7-8)$$

Thus,

$$\text{BANDWIDTH} = 2\pi f_r / Q_T \propto \sqrt{\epsilon_{r,\text{eff}}} \quad (7-9)$$

In the above relationship, the sum of the three power components is assumed to be constant and can be combined into the total power P. As can be seen from (7-9), the antenna bandwidth is directly proportional to the square root of the effective relative permittivity. In order to apply (7-8) to on-chip antennas, the expression for the effective relative permittivity will have to be modified as discussed in the previous section.

## **8.0 Patch – Simulations**

### **8.1 Introduction**

As was shown in Figure 1.4, the patch geometry is different from that of the typical microstrip on a printed circuit board. Since the majority of research done on planar antennas has been aimed towards the microstrip, there is currently very little design information available for IC antennas. Therefore, the first step in the simulation is to observe through simulation what effects the differences in IC and microstrip configurations have on the antenna performance. After that is known, the permittivities of the oxide layers will be modified and the effects on the antenna performance will be studied.

The simulations will begin with a microstrip patch antenna designed using the equations given in Section 7. These simulations will be done in Ansoft HFSS in order to display the 3D radiation patterns and get a measure of efficiency. The substrate used for this antenna will be intrinsic silicon. The input impedance curve for the antenna as a function of frequency will be plotted and it will be used to determine those frequencies where the antenna resonates. This will

be the departure point for the rest of the analysis of the rectangular patch. Following the comparison of the design results with the simulation, the substrate will be doped, and one by one the oxide layers will be added to transform the microstrip structure into one on-the-chip. At every point, the effects of each modification will be noted and discussed. The goal will be to observe if in the process of the transformation a low operating frequency can be found.

After the chip structure is complete, the permittivity of each of the oxides will be varied while the other oxide's permittivity is kept constant. The effects of the permittivity variations on the resonant frequency will be noted. The goal of these experiments will be to note what can be done to lower the operating frequency of the patch.

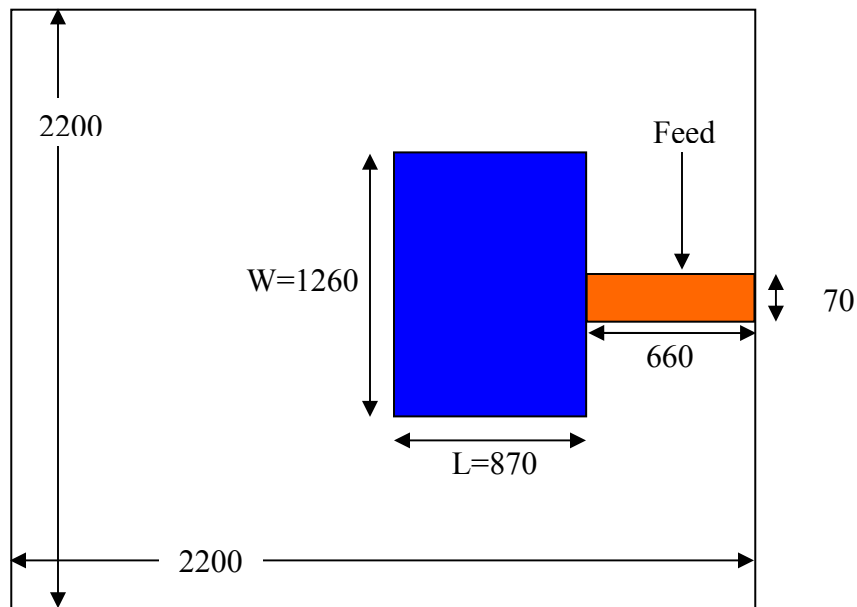


**Figure 8.1** Patch Details (all units in  $\mu\text{m}$ ).

## 8.2 Microstrip with Intrinsic Silicon

An antenna was designed using the equations given in Section 7.B to resonate at 46.9 GHz. Its dimensions are shown in Figure 8.1. The resonant frequency was chosen as 46.9 GHz in order to keep the size of the patch small enough so that other electronics can fit on the chip. It

would also provide an antenna that would not require a much larger and more expensive chip. The substrate used in the design was 300  $\mu\text{m}$ . thick undoped silicon, fixed by the available CMOS process, to preserve the same dimensions as the complete CMOS chip. The ground plane was under the substrate. The plot of the imaginary part of the impedance looking into the antenna and bypassing the feed is shown below. Bypassing the feed and looking directly into the antenna is a feature offered by both Ensemble and HFSS and it is referred to as “deembedding”. The reason for doing this is to remove the analytical complications that are added as a result of the feed.

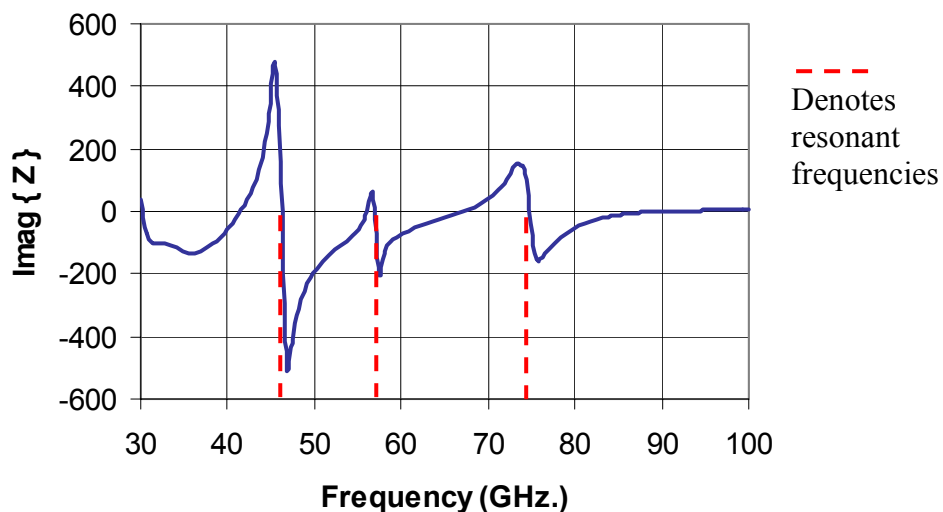


**Figure 8.2** Input Impedance

Many authors refer to the point where the imaginary impedance of the patch transitions through zero as the resonance frequency [1,7]. This is the frequency at which the patch becomes the most efficient radiator. From Figure 8.2, where the resonance points can be seen as indicated by the dashed vertical lines, the first resonant point is seen to be at 46.3 GHz., in very good agreement with the calculations. Considering the range of the simulation, an error of 600 MHz. is acceptable because it is less than 1%. This 1% is considered to be within typical analog CMOS process variations. Other resonant frequencies exist on the plot, and the antenna will

work at those frequencies as well. However, the design equations are for the dominant mode at 46.9 GHz., which achieves the best performance.

In RF work, it has been standard practice to design components that will be matched to a 50  $\Omega$  transmission line at resonance. In other words, ideally there should be no reflection of the incident voltage from the antenna at the resonance frequency. This can be better seen from the  $S_{11}$  plot which measures reflection from a transmission line with a specified characteristic impedance (in this case 50  $\Omega$ ). For details of reflection the reader is referred to Section 5.A.

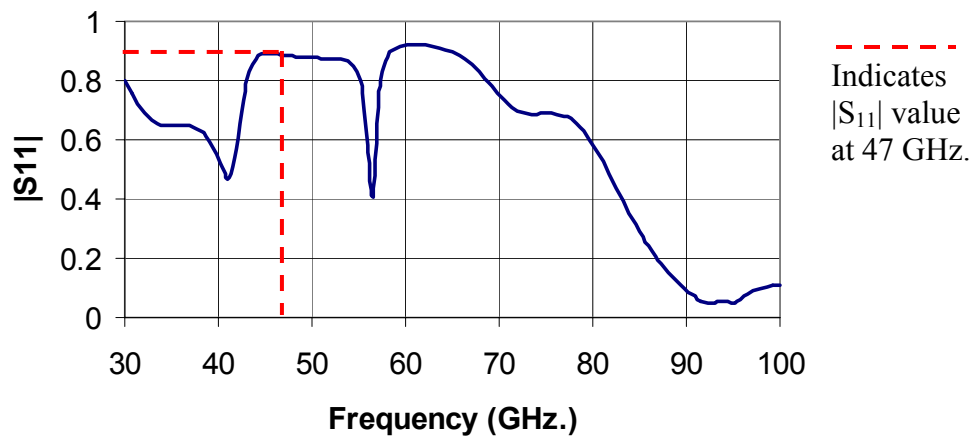


**Figure 8.3** Magnitude of Reflection Coefficient

From Figure 8.3 it appears that at 47 GHz., there is a large amount of reflection from the antenna when a 50 $\Omega$  line is connected to the antenna as can be seen by the high value of  $|S_{11}|$ . This occurs because the value of the patch impedance is not near 50 $\Omega$ . In order to get good S-parameters for the patch, an inset feed geometry must be used. The range of values for the reflection coefficient is from zero to one. By definition of the reflection coefficient [16,17], when it is zero, it means nothing is reflected and when it is one, it means everything is reflected. For an antenna at the resonance frequency, a value as close to zero as possible is preferred. That value means everything that is sent by the generator to the transmission line with characteristic

impedance  $Z_0$  is transmitted to the load, which is the antenna. This occurs because of the following relationship: Reflection Coefficient = 1 – Transmission Coefficient. When the antenna is used in the receiving mode, the situation is identical, but now the antenna serves as the generator whose impedance must be matched to the transmission line to minimize reflection.

The results of the impedance plot in Figure 8.2 describe how the power enters the antenna. The indicated points also specify at what point the antenna will be a radiator. However, they do not describe how much of the power is radiated and how much of it is lost. Nor do they describe the direction in which that power is radiated. This can be seen from the plot of the gain of the antenna which takes into account the losses.

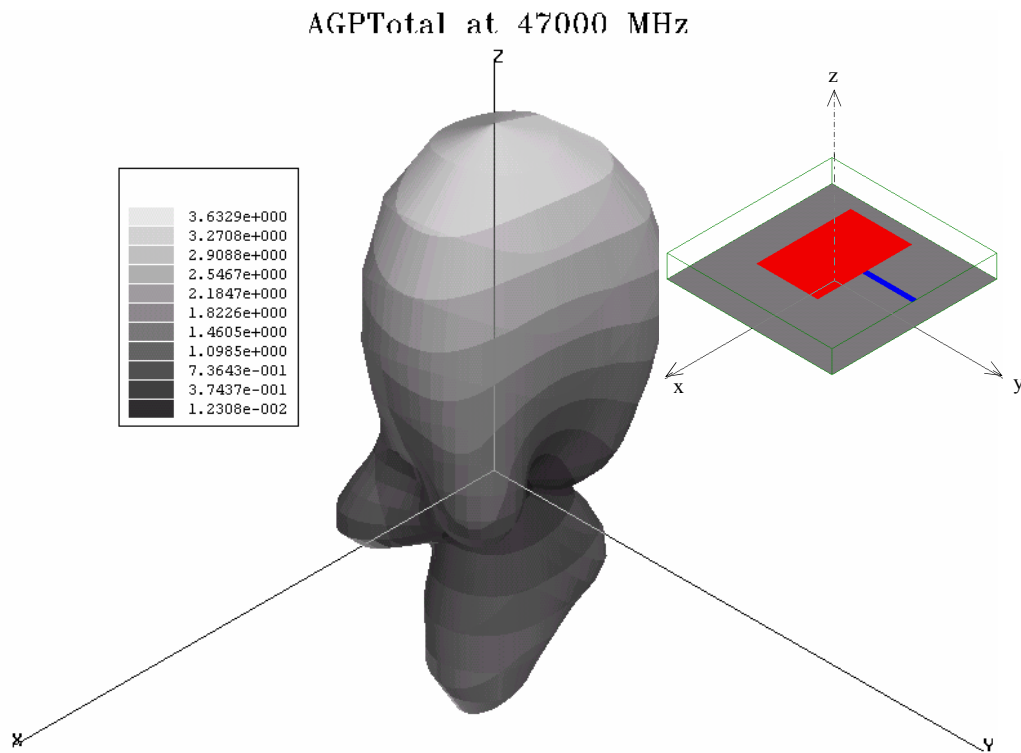


**Figure 8.4** Gain Pattern with Undoped Silicon (unitless).

From the plot of the gain, it is evident that the patch radiates mostly in the positive  $z$  direction. Also, it can be seen that this radiation is not sharply defined as noted by the lack of directivity of

the above plot. Directivity is a little better in the negative z direction (down) but little power is radiated.

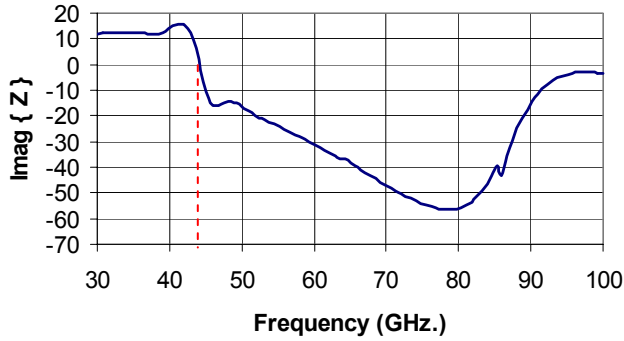
As discussed in the section on Antenna Fundamentals, gain is a measure of the power radiated in a certain direction relative to the power that would be radiated in that same direction by a lossless isotropic source. In Figure 8.4 above, regions whose gain is greater than one radiate more power than a lossless isotropic source and those where the gain is less than one radiate less. The gain can be seen from the color key code in Figure 8.4. In general, gain can be expressed as:  $\text{gain}(x,y,z) = \text{efficiency} \cdot \text{directivity}(x,y,z)$ . It follows that gain is a lumped measurement of efficiency and directivity. From a plot of gain, it is impossible to determine the efficiency without looking at a corresponding plot of directivity. This is remedied by HFSS, which provides a separate computation of the antenna efficiency. For this antenna, the computed efficiency is 95%.

### **8.3 Microstrip with Doped Silicon**

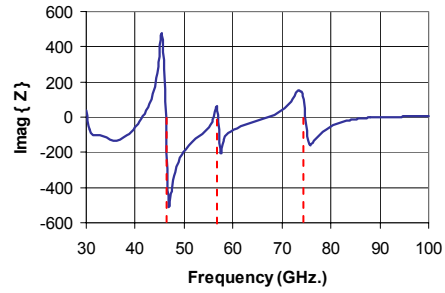
The previous simulation has been performed for silicon that is undoped. The effects of doping on conductivity were summarized in (4-1) which is repeated here:

$$\sigma = qn\mu_n + qp\mu_p \quad (8-1)$$

----- Denotes resonant frequencies



a. Silicon with Doping



b. Silicon without Doping

**Figure 8.5** Input Impedance with and without Doping

The results of the simulation that account for the non-zero conductivity, which occurs as a result of doping, are plotted in Figure 8.5. A close-up view of the point in Figure 8.5a, where the impedance crosses the zero line will reveal that the frequency at which this phenomenon occurs is 44.1 GHz. Therefore, one effect of the doping is to decrease the resonant frequency. Another effect is to eliminate all the non-dominant modes at which resonance also occurs. In this example, the doping is relatively light [ $10^{16}$  atoms/cm<sup>3</sup>], and a heavier doping [ $10^{18}$  atoms/cm<sup>3</sup>] is likely to have an even greater effect. The effects of doping also appear in the radiating properties of the antenna. As can be seen from Figure 8.6, the gain is greatly reduced over that in section 8.B. The efficiency factor of this antenna as reported by the simulator falls to 4% as can also be predicted from the low values of the antenna gain.

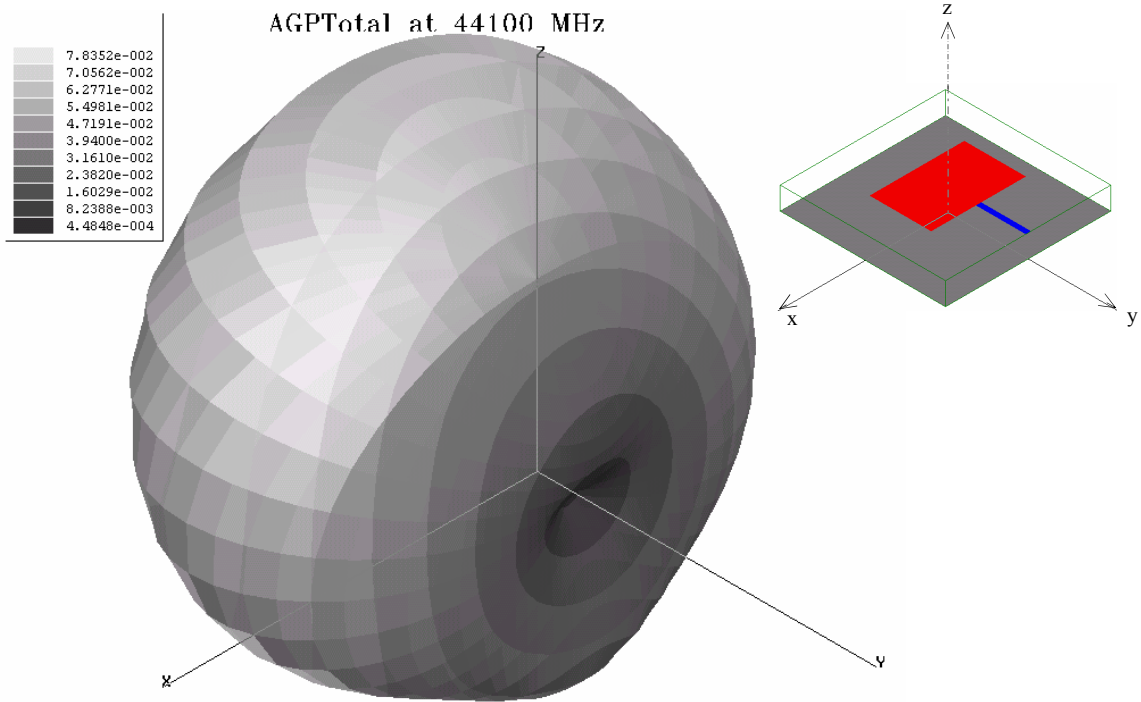


**Figure 8.6** Gain Pattern with Doped Silicon (unitless).

From this simulation, two generalizations can be inferred. The advantage gained by controlling the doping level of the substrate is the ability to control the resonant frequency, subject to the limitations described below. Undoped silicon is lossless because its conductivity is close to zero. Doping increases the conductivity of the silicon and it becomes lossy. Typically, the doping levels range from  $10^{16}$  atoms/cm<sup>3</sup>, which is considered low-doping, to  $10^{20}$  atoms/cm<sup>3</sup>, which is considered very high doping. Thus, the ability to control the resonant frequency by doping will be limited by the level of the doping. It will also be limited by the efficiency drop that occurs in the antenna because of the doping, as was demonstrated in this subsection. The main reason for these effects is the modification of the crystalline structure of pure silicon that occurs as a result of doping.

#### 8.4 Microstrip with Substrate Oxide and Doped Silicon

The progression from the microstrip to the chip where the different layers are added is continued in this section with the insertion of the oxide layer between the metal and silicon. According to the information published in literature, it is assumed that the oxide is undoped [20]. Because of this, its conductivity is assumed to be zero. The configuration of layers at this stage will be as shown in Figure 8.7 below. By simulating this configuration, it will be possible to understand what effect the addition of the substrate oxide layer has on the resonance frequency of the antenna. Understanding this effect will enable the modification of the equation for the effective relative permittivity of an antenna with a multi-layer dielectric configuration. The consequences of the addition of the superstrate oxide layer will be described in the next subsection.

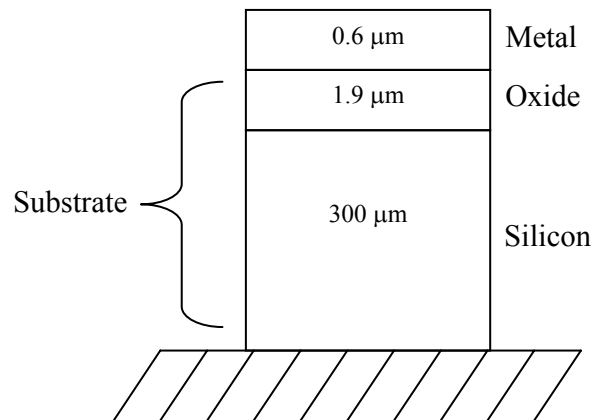


**Figure 8.7** Geometry for Simulation

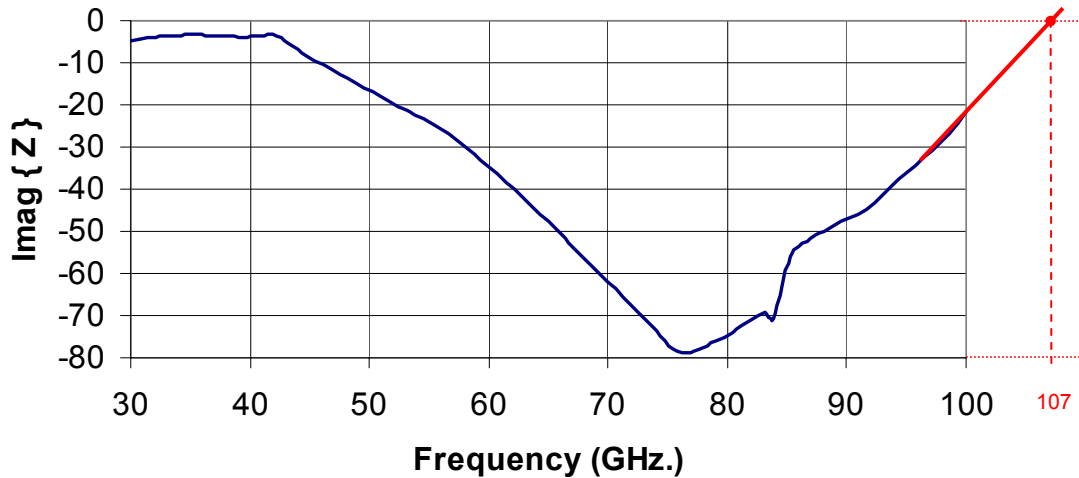


**Figure 8.8** Input Impedance with Substrate Oxide

As can be seen from Figure 8.8 this configuration of the microstrip exhibits no resonance in the frequency range of 30-100 GHz. This is apparent from the inability of the imaginary impedance to cross the zero line in Figure 8.8. Additional simulations were performed for the 1-30 GHz range and resulted in no resonance as well. From the slope of the curve it can be estimated that eventually the line with the imaginary part equal to zero is crossed but that crossing occurs at a point beyond 100 GHz., the simulation limit. This is shown in Figure 8.8 by the dash-dot line that interpolates the curve. Therefore, it is concluded that the addition of the oxide layer above the substrate deteriorates the antenna characteristics such that it can no longer be considered an antenna. Practically this means that it may be impossible to obtain a satisfactory match for this antenna to a transmission line with a real-valued characteristic impedance. This means that the absorption of energy by the antenna (as a receiving antenna) will not be very good. Another consequence of the characteristics is that the antenna appears capacitive. This is evident from a comparison of a capacitor's impedance ( $-j/\omega C$ ) with the imaginary part of the impedance in Figure 8.8. That means that the already limited energy that will be absorbed by the antenna will be stored inside the electric field of the capacitor instead of being utilized in the circuitry.

## 8.5 Chip with Sub and Superstrates and Doped Silicon

At this point the superstrate layer is added to the configuration to transform the microstrip structure to one on the chip. The layer configuration is shown below in Figure 8.9.

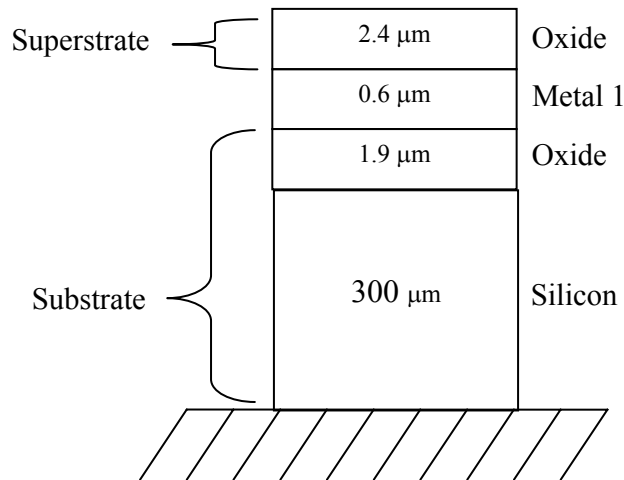


**Figure 8.9** Geometry for Simulation

The simulation results again show that the antenna does not resonate in the simulation range, but that the resonance point appears to be not too far beyond the 100 GHz. The range above 100 GHz. was not included in the simulation because of the associated time constraints. Each simulation reported here took an average time of 30 minutes. According to the author's experience, if the range had been increased to 500 GHz., the simulation time would have increased by a factor of five, to two and a half hours. Because of the absence of software features that automate the simulations, simulating such a large range would be impractical.

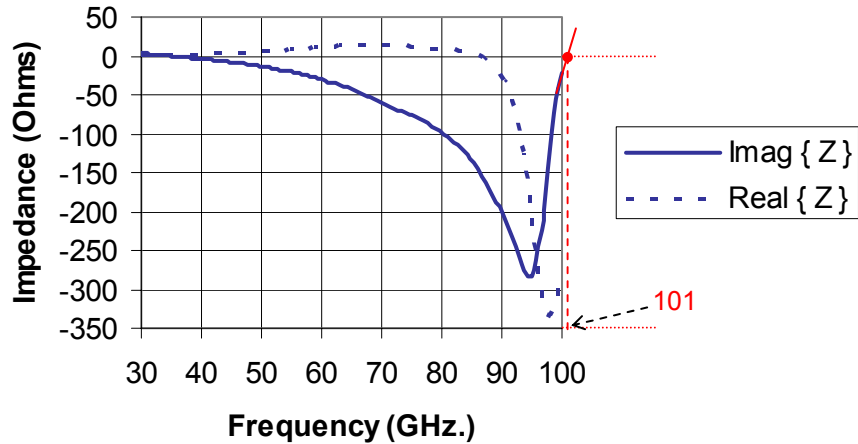


**Figure 8.10** Chip Antenna Input Impedance

A first glance at the imaginary curve in Figure 8.10 would lead to an incorrect conclusion that the antenna exhibits resonance in the 30-40 GHz range. That conclusion would be incorrect because the real curve is also zero in that frequency range. That means that the structure behaves as a short circuit, which exhibits no power loss. A short circuit by definition occurs when the real and imaginary parts of a load become zero. From ohm's law, the magnitude of the voltage drop across a load with impedance  $Z$  and through which a current  $I$  flows is  $|V|=|I||Z|$ . If  $Z$  is zero, as occurs in a short circuit, then the voltage drop must also be zero. It follows then that the power dissipated in the load, given by  $P=|V||I|$  must be zero also. Therefore, it can be concluded that in the 30-40 GHz. frequency range the structure whose impedance is shown in Figure 8.10 exhibits no power loss and does not behave as an antenna.

The results shown in Figure 8.10 are very similar to those in Figure 8.8. In both cases the resonance does not occur in the simulation range. Gain was not plotted for these two cases because its plot would not make any sense. Also it is not clear at which frequency this plot should be made. These results show that a patch on a chip will not exhibit resonance if the dielectric layers are in their standard states as shown in Figure 8.9. Some modifications to those

layers must be made in order to have an antenna that will resonate in the 30-100 GHz. frequency range.

### 8.6 Variation of Superstrate Oxide Permittivity

This section presents the results of the variation of superstrate permittivity. The permittivity was varied from 0.4 to 16.4, in increments of 0.5, representing the range of most dielectric materials. The resonant frequency was determined as before at the point where the imaginary part of the impedance crossed the zero line. Several permittivity values resulted in no resonance in the simulation range. Those permittivities that resulted in resonance are indicated by the square markers on the plot below.

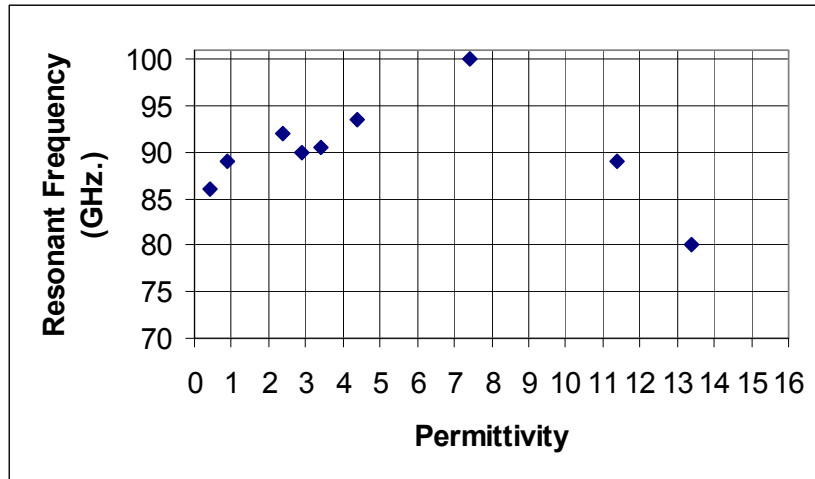


**Figure 8.11** Resonant Frequency as a Function of Superstrate Permittivity

It can be seen from Figure 8.11 that the lowest resonant frequency can be obtained by having a superstrate of a very small permittivity or a very large one. For instance, with a low permittivity of 0.4 a resonant frequency of 86 GHz. results. A high permittivity value of 13.4 also produces a low resonant frequency of 80 GHz. A plot of the curve with a high permittivity value of 13.4 is shown in Figure 8.12. These results suggest a relationship similar to (7-3a) for an effective

relative permittivity, and it is not a linear relationship. In other words, from the results it appears that the dependence of the effective relative permittivity on the relative permittivity of the superstrate is not linear.

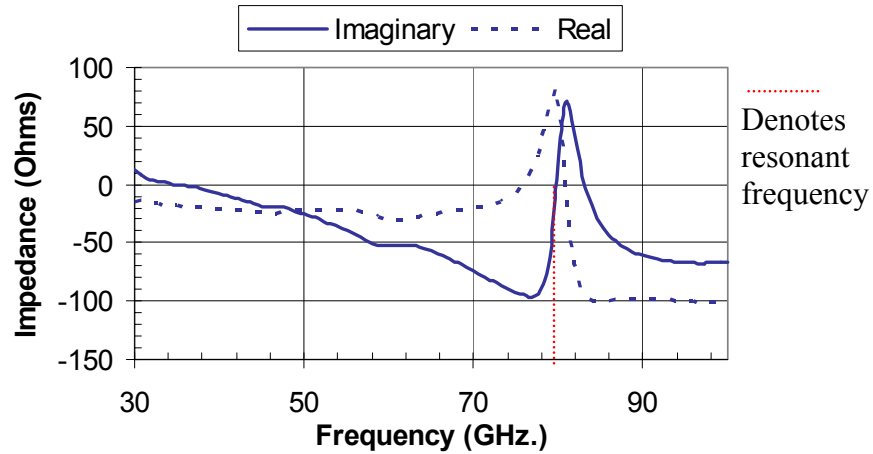


**Figure 8.12** Input Impedance with Superstrate Permittivity of 13.4

### 8.7 Variation of Substrate Oxide Permittivity

This section presents the results of the change in permittivity of the substrate oxide. This is the oxide that is placed on top of the silicon. The proper name of this oxide is silicon dioxide. According to literature [20], it is assumed here that this material is undoped and, therefore, its conductivity is zero.

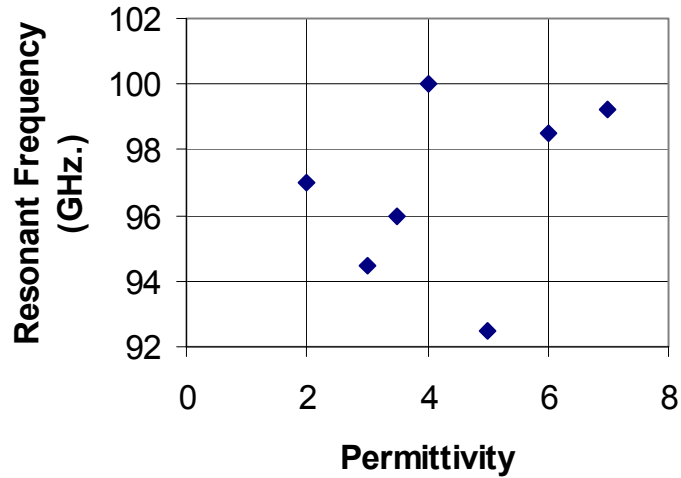


**Figure 8.13** Resonant Frequency as a Function of Substrate Oxide Permittivity

The results of simulations where the permittivity was varied are shown in Figure 8.13. The lack of linearity of the graph suggests that the permittivity of the substrate oxide is not a very good parameter for robust control of the resonant frequency of the antenna. An expression for the dependence of the effective relative permittivity on the substrate oxide permittivity could be derived but it would be very complicated and not useful due to the sensitivity of the result in light of potential process variations. Comparison of Figure 8.11 with Figure 8.13 indicates that the range of frequencies that can be controlled (92 GHz. to 100 GHz.) by the substrate oxide is nearly half of the range that can be controlled by the superstrate oxide. A plot of the curve for a permittivity value of 5.0 is shown in Figure 8.14 for comparison with Figure 8.12.

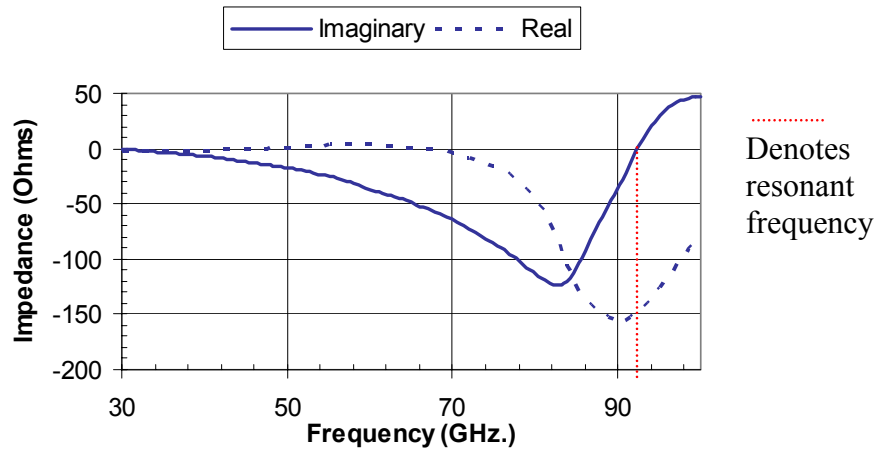


**Figure 8.14** Input Impedance with Substrate Permittivity of 5.0

## 9.0 Square Spiral – Simulations

### 9.1 Introduction

Another type of on-chip antenna, designed to operate in a lower frequency range than the patch, was investigated next. This antenna had been designed previously using the software tool ASITIC [14] discussed elsewhere. It is a single-turn [14] square spiral designed with a goal to resonate in the 1-1000 MHz. range. Just as in the patch case, resonance is achieved when the imaginary part of the input impedance approaches zero and the real part is maximum.

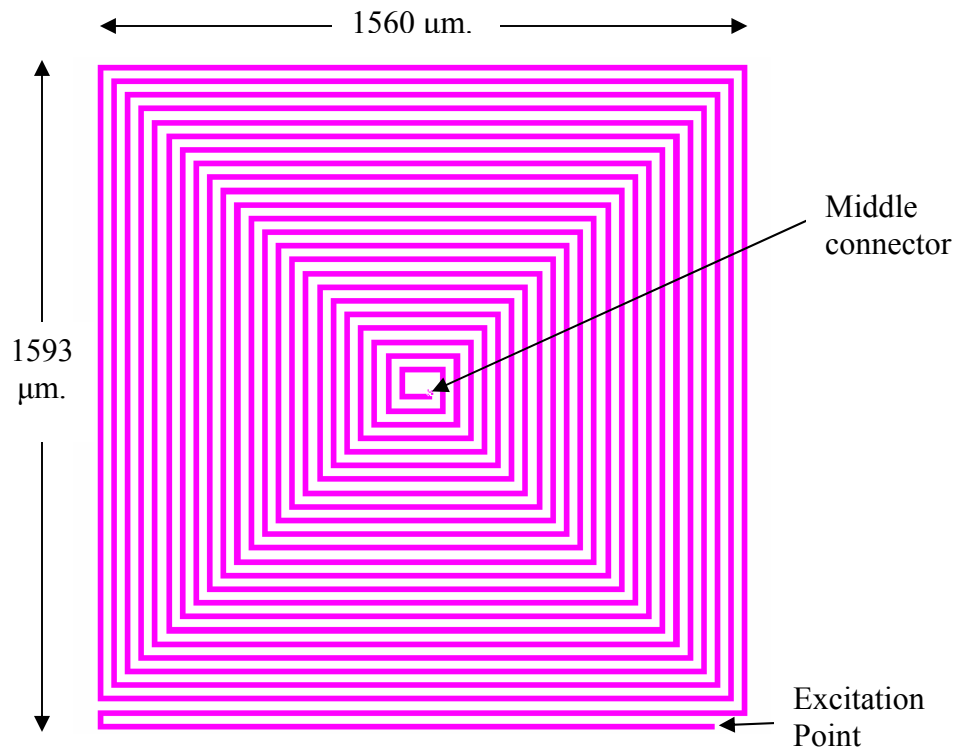


**Figure 9.1** Square Spiral Top View.

To achieve the design goal, the spiral antenna was designed on metal 2, the top metal layer. This layer has a lower sheet resistance than metal 1 and, therefore, conduction losses are reduced. This configuration is shown in the figure below.

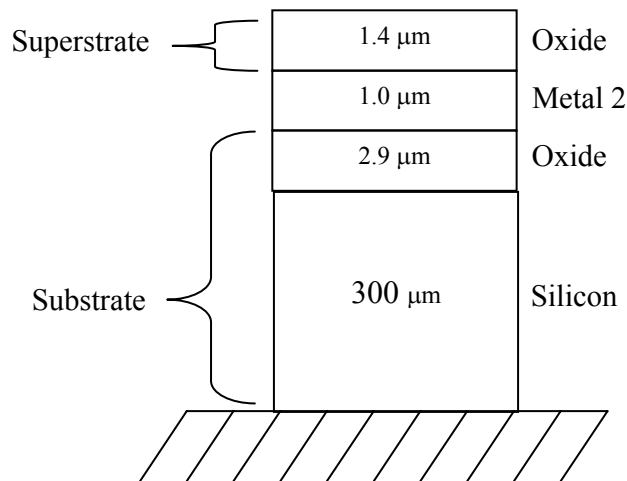


**Figure 9.2** Spiral Geometry Side View

With the excitation point as shown in Figure 9.1 two possible operating modes exist. In the first mode, the middle connector of the spiral is connected to ground with a vertical via and in the

second mode one the middle is left floating. The via is displayed in Figure 9.3. In both cases, the signal is applied between the excitation point and ground. Note that although the middle antenna contact may not be grounded directly, the parasitic capacitance between the spiral traces and grounded substrate does provide a return path for the current.

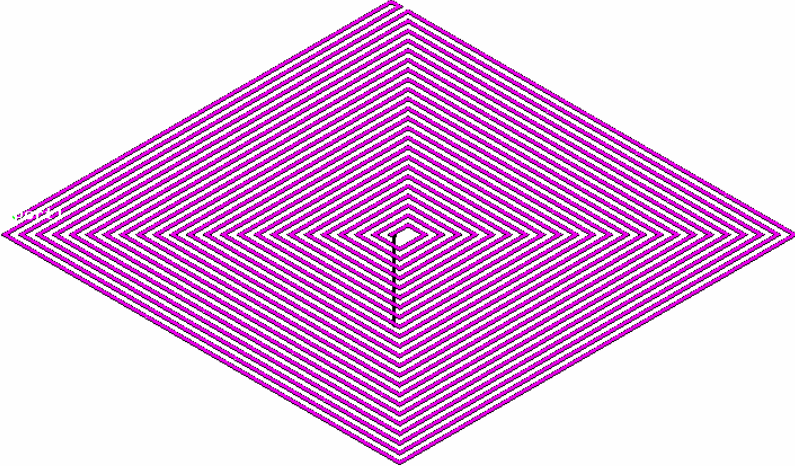


**Figure 9.3** Spiral Antenna with a Via to Ground

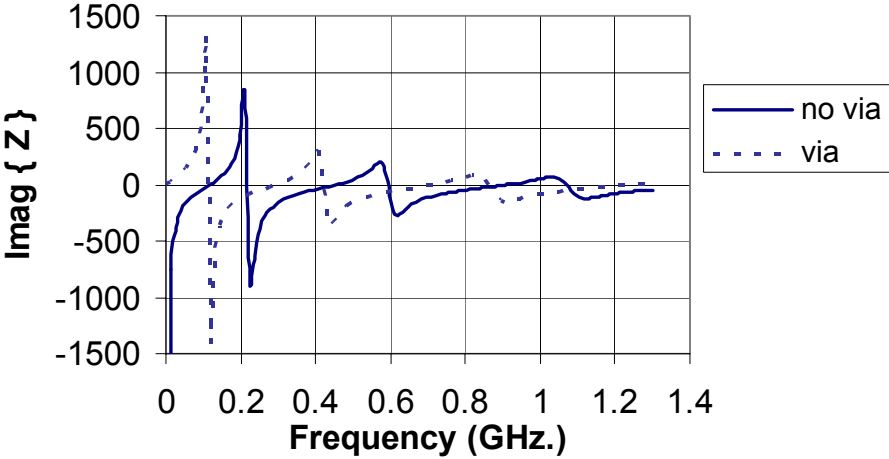


**Figure 9.4** Effect of Middle Via

The first thing that can be observed from Figure 9.4 is that there are multiple resonant points. The condition of resonance is that the imaginary part of the impedance is zero and the real part is very large. Based on this, there are three possible resonant points for each of the two cases

shown in Figure 9.4. For the no via case, they are at 217, 593, and 1070 MHz. This is emphasized in Figure 9.5, which is shown below. The imaginary part of the input impedance curve is zero at other frequencies as well, but at those frequencies the real part is zero or is very small. These points are not considered resonances, as discussed in Section 8.E.

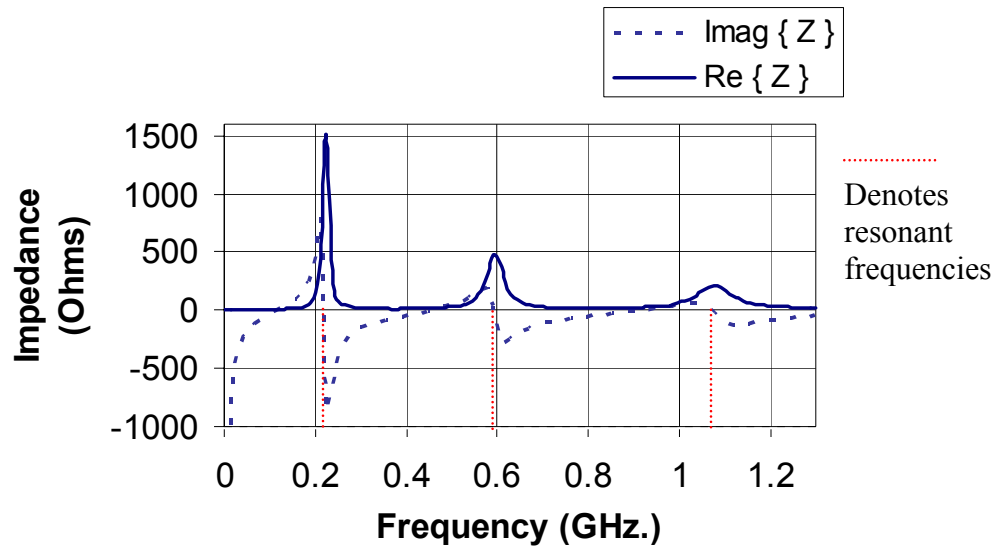


**Figure 9.5** Input Impedance of Spiral Antenna (no via).

As can be observed from Figure 9.4, the consequence of adding a via to the middle connection of the spiral is a shift of the input impedance curve. As a result, all the resonant points are shifted to a lower frequency. In the following discussion, the location of each of these three resonant points for the no via case will be observed as the dielectric parameters are varied. The other case (with via) will not be used for evaluation because the results can be predicted from Figure 9.4. Each point will be assigned its own curve named freq1, freq2, and freq3, corresponding to each resonant frequency in Figure 9.5. Again, the goal of the following experiments will be to see what can be done to the dielectric layers to lower the operating frequency of the spiral.

Another interesting observation can be made for the DC case of zero Hz. When there is no via connection, the spiral's reactance asymptotically approaches a very large negative value at DC. Thus, the behavior at DC is characteristic of that of a capacitor. However, when a via is added, the spiral behaves as a resistor because the imaginary part becomes zero and, therefore, there is no reactance.

## 9.2 Variation of Substrate Oxide Permittivity

An analysis similar to that carried out in the last chapter was performed for the square spiral. The permittivity of the substrate and superstrate oxides was varied and the effect of the variation on the resonant frequencies of the antenna was observed. Figure 9.6 shows the results of that analysis. As can be seen from this figure, the variation of the permittivity of the substrate oxide has a similar effect on all the resonant frequencies of the spiral. However, the first peak shows the least sensitivity and the last peak shows the most sensitivity.

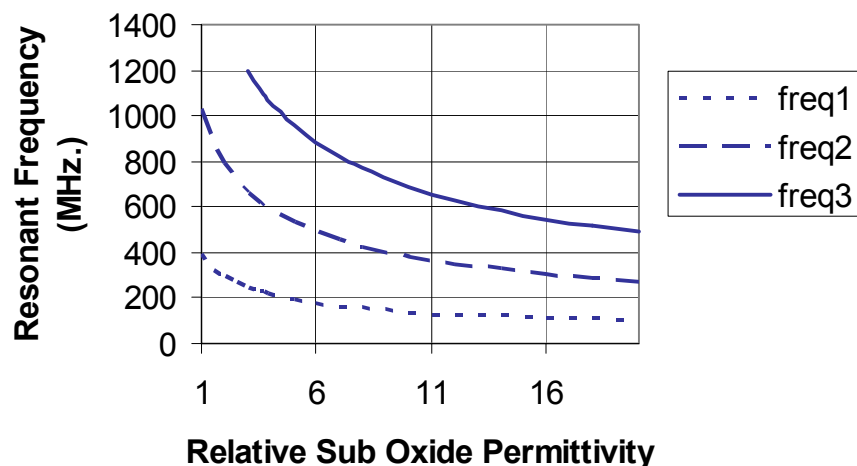


**Figure 9.6** Effects of Changing the Substrate Permittivity.

The lines of Figure 9.6 represent the migration of the resonance points of Figure 9.5 as the relative permittivity of the sub oxide layer is varied.

### 9.3 Variation of Superstrate Oxide Permittivity

Figure 9.7 shows the changes in resonant frequency that occur as a result of variations in the permittivity of the superstrate oxide. Again, these lines show the migration of the resonance points of Figure 9.5 as the permittivity of the super oxide layer is varied.

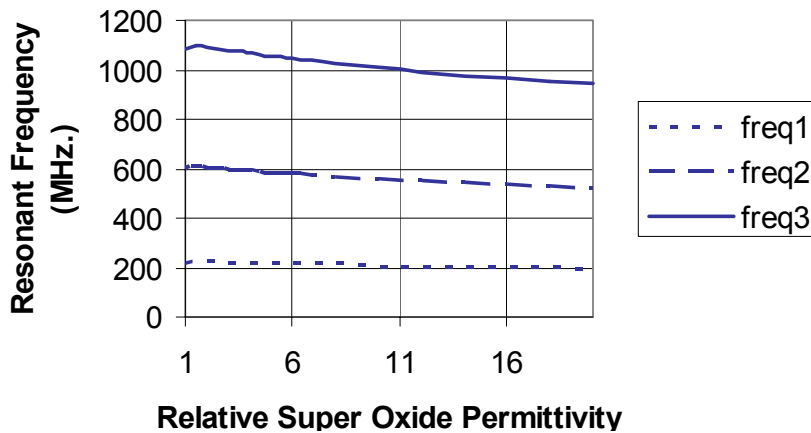


**Figure 9.7** Effects of Changing the Superstrate Permittivity

The results of Figure 9.7 show that all the resonant frequencies exhibit a much smaller sensitivity to the superstrate permittivity, compared to the substrate permittivity. This is because the spiral antenna has a low radiating efficiency. This means that its operation is primarily determined by the parasitic capacitance between it and ground. This capacitance is typically given by [14] as:

$$C = \frac{\epsilon A}{h} \quad (9-1)$$

where  $\epsilon$  is the effective permittivity of all the layers between the capacitor (spiral) and ground,  $A$  is the area of the capacitor, and  $h$  is the height of the layers between the capacitor and ground.

This explains why the spiral's resonant frequency is primarily dependent on the effective permittivity of the substrate. The dependence on the permittivity of the superstrate is not as pronounced because the superstrate permittivity will affect the wave propagation characteristics

such as its frequency, but it won't affect the operation of the antenna. Also, both Figure 9.6 and Figure 9.7 demonstrate that the third frequency has the largest sensitivity of the three.

A comparison of Figures 9.6 and 9.7 leads to the conclusion that the permittivity of the substrate oxide plays a greater role than the permittivity of the superstrate oxide in determining the resonant frequency of the spiral. This can be useful to the designer in determining in which layer the permittivity must be adjusted in order to reach a design goal of a certain resonant frequency.

## **10.0 Summary and Conclusions**

Design data for the rectangular patch has been presented and analyzed. The design approach was to present the equations for the microstrip and then show how to adapt those equations for the case of the on-chip patch. The dependence of the patch resonant frequency on the antenna's dimensions and on the effective relative permittivity was shown. The major modification that must be made to the equations is to calculate the effective relative permittivity for the antenna on a chip. This is a straightforward calculation for the microstrip antenna, but it is a much more involved calculation for an antenna on a chip. Based on the results of this thesis, future research needs to be performed to establish a tractable mathematical relationship.

Following the design information, simulations of the rectangular patch were performed. The simulations had several goals. The first goal was to show the effect of adding each layer as the microstrip antenna was transformed into one on a chip. This effect was to decrease the antenna's efficiency, reduce the number of resonant frequencies, and some cases resulted in the disappearance of resonant frequencies from the simulation range. The second goal was to demonstrate what happens to the antenna's operating frequency as the relative permittivity of

some dielectric layers is varied. This effect was great enough to have a significant impact on the operating frequency.

The initial microstrip case with the patch placed on top of an undoped silicon substrate showed very good agreement with the calculated resonance point of 47 GHz. and also very high radiation efficiency. This suggested that the simulation setup in the software was correct and validated the setup for the experiments to follow, for which calculated values were not available. This configuration also resulted in the presence of a multitude of other resonance frequencies, due to the lossless ness of the silicon substrate. As the conductivity of silicon was modified to account for the practical scenario of doping, the multiple resonance points were no longer observed and the 47 GHz. point was shifted to 44.1 GHz. This configuration also resulted in an attendant severe decrease of the efficiency of the antenna. Subsequent additions of the substrate and superstrate oxides altered the characteristics of the patch antenna to a very high degree such that it could no longer be considered an antenna in the 30-100 GHz. simulation range.

At this point, the patch was configured with all the layers that exist on the chip and it exhibited no resonance. Using the results of the simulation, it was shown that the resonance frequency could be controlled to a limited degree by varying the superstrate permittivity. Values in the low (0-3) and high (10-14) ranges of the permittivity had the greatest impact on the frequency of operation. The maximum shift of 20 GHz. was achieved for a permittivity of 13.4. Variation of the substrate permittivity also resulted in changes to the frequency of operation, but those changes were not as predictable and the range of frequencies was decreased. Similar research done by Jackson and Alexopoulos [4] suggests that it may be possible to affect the resonant frequency by simultaneously changing the permittivities of the substrate and superstrate

of certain geometries. This type of analysis was not considered here and future investigation in this direction may also be performed.

To illustrate the effects of the permittivity changes on an antenna designed to work at lower frequencies, a (nearly) square IC spiral was considered. This is a spiral antenna designed to operate in the 1-1000 MHz. frequency range. Simulations demonstrated that the operating frequency (resonance) decreases as a result of increasing either the substrate or the superstrate permittivity. The substrate permittivity had the greatest impact on the frequency, which was varied by up to 700 MHz. In contrast, the superstrate permittivity had a much smaller impact and could cause a maximum shift in frequency by only 150 MHz. This is because the substrate permittivity dominates the operation of the spiral due to its low efficiency. The simultaneous variation of the substrate and superstrate oxide permittivities was not considered here but the results of the spiral suggest that research in this direction may be possible.

A comparison of the patch and the spiral antennas shows that the range of frequencies that can be controlled by changing the relative permittivity appears to increase with the resonant frequency of the antenna. In the low frequency spiral, the maximum range of frequencies was 700 MHz. while for the high frequency patch it was 20 GHz. This shows an increase in the frequency range by nearly 30 times as the frequency is increased, indicating a possible accuracy limitation at high frequencies. The range therefore is a function of frequency. This has an effect on the frequency tolerances and should be accounted for in the antenna design. The tolerances come into play because the relative permittivities of the substrate and superstrate materials are not exact and can possibly vary from one chip to the next. The reason this must be accounted for is that at higher frequencies, even small deviations from the normal permittivity can have a significant impact on the operating frequency of the antenna.

Furthermore, in all cases, a high value of the superstrate permittivity resulted in a reduction of the operating frequency of the antennas studied. Thus, it is recommended that the substrate material remain the same, but the superstrate material may be replaced with one having a permittivity at least as high as silicon (11.9). Based on the results shown in this thesis, this configuration will result in a maximum reduction of the operating frequency of the patch antenna, and to a smaller degree a reduction of the operating frequency of the spiral.

Both antennas have shown that their resonance frequency(s) respond well to the variation of the permittivities of the substrate and/or the superstrate layers. The responses tend to follow a predictable path for which mathematical relationships may be derived. This is a suggested area for future research. These mathematical relationships can then be used to modify the design equations of the antennas to account for the transition from the microstrip to the on-chip design.

## **BIBLIOGRAPHY**

## BIBLIOGRAPHY

- [1] C. A. Balanis, *Antenna Theory: Analysis and Design*. New York: Wiley, 1997.
- [2] D. M. Pozar, "Microstrip Antennas," *Proceeding of the IEEE*, vol. 80, no. 1, pp. 79-91, January 1992.
- [3] D. H. Schaubert, D. M. Pozar, and A. Adrian, "Effect of Microstrip Antenna Substrate Thickness and Permittivity: Comparison of Theories with Experiment," *IEEE Transactions on Antennas and Propagation*, vol. 37, no. 6, pp. 677-682, June 1989.
- [4] N. G. Alexopoulos and D. R. Jackson, "Fundamental Superstrate (Cover) Effects on Printed Circuit Antennas," *IEEE Transactions on Antennas and Propagation*, vol. AP-32, no. 8, August 1984.
- [5] J. R. James, P. S. Hall, and C. Wood, *Microstrip Antenna Theory and Design*. New York: IEE, 1981.
- [6] K. Wong, *Design of Nonplanar Microstrip Antennas and Transmission Lines*. New York: Wiley, 1999.
- [7] J. D. Kraus, *Antennas*. New York: McGraw-Hill, 1950.
- [8] M. N. O. Sadiku, *Elements of Electromagnetics*, 2<sup>nd</sup> ed., Philadelphia: Saunders College Publishing, 1994.
- [9] M. H. Mickle, D. Gorodetsky, L. Mats, L. Neureuter, M. Mi, and C. Taylor, (2001) "Apparatus for Energizing a Remote Station and Related Method," Continuation in Part to US Patent 6,289,237, Serial Number 09/951,032, March 2002.
- [10] C. Emahiser, "An Investigation of a Radio Frequency Energy Detector Using Microstrip Technology," M.S. Thesis, University of Pittsburgh, 1999.
- [11] <http://www-bsac.eecs.berkeley.edu/~pister/SmartDust/>
- [12] <http://www.janet.ucla.edu/WINS>
- [13] [http://www-mtl.mit.edu/~jimj/project\\_top.html](http://www-mtl.mit.edu/~jimj/project_top.html)

- [14] A. M. Niknejad and R. G. Meyer, *Design, Simulation and Applications of Inductors and Transformers for Si RF ICs*. Boston: Kluwer Academic Publishers, 2000.
- [15] J. M. Rabaey, M. J. Ammer, J. L. da Silva Jr., D. Patel, and S. Roundy, "PicoRadio Supports Ad Hoc Ultra-Low Power Wireless Networking," *IEEE Computer*, vol. 33, no. 7, pp. 42-48, July 2000.
- [16] Hewlett Packard Corporation, Application Note 1287-1, "Understanding the Fundamentals of Vector Network Analysis."
- [17] Hewlett Packard Corporation, Application Note 95-1, "S-Parameter Techniques for Faster, More Accurate Network Design."
- [18] C. A. Balanis, *Advanced Engineering Electromagnetics*, John Wiley & Sons, New York, 1989.
- [19] W. H. Hayt, Jr. and J. E. Kemmerly, *Engineering Circuit Analysis*, McGraw-Hill, New York, 1993.
- [20] P. V. Zant, *Microchip Fabrication*, McGraw-Hill, New York, 1997.